Mastering of the terahertz (THz) spectral range has motivated intensive studies aimed at developing applications of THz radiation. Spectroscopy is one of them, as molecular absorption lines corresponding to the vibrational and/or rotational frequencies belong to the THz range. Subwavelength sample thicknesses impose great difficulties to conventional THz spectroscopy, yet sensing of such samples is essential. Potentialities of thin film THz spectroscopy are considerably enlarged if a sample is probed by surface plasmon-polaritons (SPP) - the complex of an evanescent EM wave coupled to a wave of free charges propagating nonradiatively along the surface. The book describes principles and achievements in the field of THz SPP spectroscopy. Two concepts (absorption and amplitude-phase) of the method are described. Designs of static and dynamic SPP spectrometers, techniques for determining the dielectric function of metals via measured characteristics of SPP, interferometers able of measuring the SPP complex refractive index and principles of dispersive THz SPP Fourier-transform spectroscopy are considered.

Alexey Nikitin

Alexey K. Nikitin, Dr.Sc.: Studied Radio Physics at the Russian University of Peoples' Friendship. Leading Scientist of the Scientific and Technological Center for Unique Instrumentation of Russian Academy of Sciences, Moscow.

978-3-8465-8738-6

Alexey Nikitin
Anatolii Kiryanov
Boris Knyazev

Principles of terahertz surface plasmon-polariton spectroscopy

Concepts, Methods, Devices

LAP LAMBERT Academic Publishing

Alexey Nikitin
Anatolii Kiryanov
Boris Knyazev

Principles of terahertz surface plasmon-polariton spectroscopy

Alexey Nikitin
Anatolii Kiryanov
Boris Knyazev

Principles of terahertz surface plasmon-polariton spectroscopy

Concepts, Methods, Devices

LAP LAMBERT Academic Publishing

Impressum / Imprint
Bibliografische Information der Deutschen Nationalbibliothek: Die Deutsche Nationalbibliothek verzeichnet diese Publikation in der Deutschen Nationalbibliografie; detaillierte bibliografische Daten sind im Internet über http://dnb.d-nb.de abrufbar.

Bibliographic information published by the Deutsche Nationalbibliothek: The Deutsche Nationalbibliothek lists this publication in the Deutsche Nationalbibliografie; detailed bibliographic data are available in the Internet at http://dnb.d-nb.de.

Coverbild / Cover image: www.ingimage.com

Verlag / Publisher:
LAP LAMBERT Academic Publishing
ist ein Imprint der / is a trademark of
AV Akademikerverlag GmbH & Co. KG
Heinrich-Böcking-Str. 6-8, 66121 Saarbrücken, Deutschland / Germany
Email: info@lap-publishing.com

Herstellung: siehe letzte Seite /
Printed at: see last page
ISBN: 978-3-8465-8738-6

CONTENT

I. Introduction

The terahertz (THz) range of electromagnetic radiation is situated between infrared (IR) and millimeter spectral ranges that are waves having wavelength λ ranging from 30 μm to 300 μm corresponding to wavenumbers σ varying from 330 cm^{-1} to 33 $см^{-1}$ or to frequencies ν from 10 THz to 1 THz[1].

Emission (absorption) of THz electromagnetic waves accompanies many physical-chemical processes. However up to 80-th scientists did not have rather powerful sources of THz-radiation, except for lasers functioning on water and methanol vapor generating at widely spaced discreet frequencies. The situation drastically changed in the middle of 80-th, when a number of *free-electron lasers* (FEL) capable to generate intense monochromatic radiation of gradually tunable frequency were built and became accessible for scientific community[2].

Molecular spectroscopy came to be one of the most important applications of FEL THz radiation, as many molecular absorption lines corresponding to vibrational and/or rotational molecular frequencies belong to the THz spectral range.

Molecules on solid surfaces constitute a new set of molecular systems. It is practically impossible to apply conventional spectroscopic methods to such systems because of small number of molecules in them, usually an adsorbate monolayer contains 10^{15} molecules per square centimeter and this is 10^4-10^6 times less than sampled in traditional spectroscopic experiments. The traditional optical methods for testing surfaces of metals are of low efficiency as the reflectivity of metals in far IR is close to unity. This, in particular, is confirmed by the absence of experimental data on the optical constants of metals in the THz range in fundamental handbooks[3].

The potentialities of thin film spectroscopy were considerably enlarged when they began to use samples (surfaces of solids) as a part of the optical resonator where the probing radiation excites *surface plasmon-polaritons* (SPP)[4].

---

[1] Zhang X.-C., Xu J. Introduction to THz Wave Photonics // Springer Sci.+Business Media, 2010. – 246 p.
[2] Marshall T.C. Free-electron lasers. MacMillan: New York, 1985. - 240 p.
[3] Handbook of Optical Constants of Solids. Ed. by E. D. Palik /Academic, San Diego, 1998. – 804 p.
[4] Surface polaritons. Surface electromagnetic waves at surfaces and interfaces. Ed. by V.M. Agranovich and D.L. Mills (Amsterdam, New-York, Oxford, 1982). - 587 p.

Surface plasmon-polaritons are the complex of an inhomogeneous evanescent *p*-polarized electromagnetic wave coupled to a wave of density of free electrons propagating non-radiatively along the conductor/dielectric interface. Those interested in detailed description of nature, methods of excitation and applications of SPP may refer to a number of brilliant reviews and monographs on SPP subject matter published nearly two decades ago[4,5] and recently[6,7].

SPP field has its maximum at the sample surface and decreases exponentially with moving away from it. This is the main reason why characteristics of SPP, such as propagation length L, phase velocity ϑ, and penetration depth δ in the dielectric (predominantly, air) are very sensitive to optical properties of the conducting surface and its transition layer. Having determined the SPP complex refractive index $\kappa=\kappa'+i\cdot\kappa''$ via measured $L=(2k_o\cdot\kappa'')^{-1}$ and $\vartheta=C/\kappa'$ (here $k_o=2\pi/\lambda$, C - speed of light in free space), one can calculate two unknown parameters of the film at the surface or the optical constants of the metal substrate. Therefore SPP are effectively used in optical sensing[8], microscopy[9, 10, 11] and spectroscopy of metal surfaces as well as for their refractometry[12, 13, 14], bringing good results in the visible and middle infrared spectral ranges.

As for the far IR spectral range, specifically for the THz region, the understanding of the SPP phenomenon, let alone its use, is far from being complete. The cause is not only the recent lack of well-developed sources and detectors of THz radiation but

[5] Raether H. Surface Plasmons on Smooth and Rough Surfaces and on Gratings // Springer-Verlag, Berlin, Heidelberg, 1988, v.111 of Springer-Verlag Tracts in Modern Physics. – 133 p.
[6] Novotny L., Hecht B. Principles of nano-optics // Cambridge university press, Cambridge, 2006. - 382 p.
[7] Maier S.A. Plasmonics: Fundamentals and Applications // Springer Science+Business Media LLC, 2007.– 223 p.
[8] Homola J., Yee S.S., Gauglitz G. Surface plasmon resonance sensors: review // Sensors and Actuators (B), 1999, v.54, p.3–15.
[9] Yeatman E.M., Ash E.A. Surface plasmon microscopy // Electronics Letters, 1987, v.23(20), p.1091-1092.
[10] Nikitin A.K., Tischenko A.A. Surface electromagnetic waves phase microscopy // Technical Physics Letters, 1991, v.17(11), p.76-79. (In Russian)
[11] Somekh M.G. Surface Plasmon and Surface Wave Microscopy // Optical Imaging and Microscopy, Springer Series in Optical Sciences, Springer-Verlag, Berlin Heidelberg, 2007, v.87, p.347-397.
[12] Kretschmann E. Die Bestimmung optischer Konstanten von Metallen durch Anregun von Oberflachenplasmaschwingungen // Zeitschrift fur Physic, 1971, Bd.241, s.313-324.
[13] Gu J.H., Cao Z.Q., Shen Q.S., and Chen G. Determination of thickness and optical constants of thin metal films with an extended ATR spectrum // J. Phys. (D): Appl. Phys., 2008, v.41, 155309.
[14] Lafait J., Abeles F., Theye M.L., Vuye G. Determination of the infrared optical constants of highly reflecting materials by means of surface plasmon excitation – application to *Pd* // J. Physics (F): Metal Physics, 1978, v.8(7), p.1597-1606.

the specific properties of THz SPP. These peculiarities become obvious when following main SPP characteristics evolution with λ increase from visible to THz ranges. Example of this evolution for a bare aluminum surface bordering air is presented in Table 1[15]. Here $\varepsilon_1=\varepsilon_1^{'}+j\varepsilon_1^{''}$ is the complex dielectric functions of aluminum; δ_1 and δ_2 are the SPP field penetration depths into the metal and vacuum, accordingly.

Table 1

λ, μm	$\varepsilon_1^{'}$	$\varepsilon_1^{''}$	κ′	κ″	δ_1, μm	δ_2, μm	L, cm
0.6	-56.6	21.4	1.007808	0.003000	0.012	0.76	0.002
1.0	-91.3	26.1	1.005100	0.001467	0.016	1.57	0.005
5.0	-2287	843	1.000193	0.000071	0.017	40.5	0.561
10.3	-7793	4905	1.000046	0.000029	0.018	171	2.833
20.0	-17925	17845	1.000014	0.000014	0.022	602	11.4
32.0	-32655	42848	1.000006	0.000007	0.024	1521	34.5
100.0	$-2\cdot10^5$	10^5	1.000002	0.000001	0.035	7905	795

One can see that as the wavelength increases SPP acquires more pronounced photon character, namely at THz frequencies (λ≥30 μm) its phase velocity approaches the speed of light, the field penetration depth in vacuum δ_2 increases up to centimeters, while propagation length L reaches almost 10 meters. So the peculiarities of THz SPP as compared with their visual counterparts may be summarized as follows: 1) their refractive index κ′ exceeds that of light in the surrounding medium n only by hundredths or even thousandths of a percent; 2) their field penetrates in air (or vacuum) to a distance δ≥100λ; 3) as small as hundredths to thousandths of the their total field energy is transported in the metal, which results in small absorption of THz SPP and their vast propagation length L, reaching meters.

A decade ago a revolution seemed to take place in the THz plasmonics. It was suggested to use the time-domain spectroscopy (TDS) approach and photo conduc-

[15] Zhizhin G.N., Nikitin A.K., Bogomolov G.D., Zavyalov V.V., Jeong Y.U., Lee B.C., Park S.H., Cha H.J. Absorption of surface plasmons in "metal-cladding layer-air" structure at terahertz frequencies // Infrared Physics & Techn., 2006, v.49(1-2), p.108-112.

tive antennas (PCA) to excite and detect THz SPP[16]. It looked very attractive to span the whole THz band in one-procedure measurements determining both amplitude and phase spectra of the SPP. In their pioneer TDS experiments on SPP, Saxler J. and coworkers made an attempt to establish the SPP amplitude spectrum in the range from 0.2 to 2.4 THz[17]. Since that time a number of researchers used the TDS technique to study THz SPP on plane and cylindrical surfaces brining abundance of experimental data intricate for spectroscopic interpretation as the complex instrumental function acquires additional unknown complex factors, which take into account the transformation efficiency of bulk radiation into SPP and vice versa, as well as the dispersion of the phase shift of radiation components at these transformations; let alone the 2π ambiguity in phase shift for the spectrum components.

Nevertheless nowadays it may be stated that all the basic techniques and elements required for the THz SPP metrology have been developed and the time for putting it into practice has come. Here we introduce achievements and problems in the field of SPP spectroscopy at THz frequencies.

[16] Lozovik Yu.E., Merkulova S.P., Nazarov M.M., Shkurinov A.P. From two-beam surface plasmon interaction to femtosecond surface optics and spectroscopy // Physics Letters (A), 2000, v.276, p.127–132.
[17] Saxler J., Rivas J.G., Janke C. et al. Time-domain measurements of surface plasmon polaritons in the terahertz frequency range // Phys. Rev. (B), 2004, v.69, 155427.

II. Absorption THz spectroscopy of metal surfaces by SPP

II.1. *Features of THz SPP excitation by bulk waves*

The most common way of generating THz SPP is an interaction of bulk radiation with a conducting surface. Due to very large penetration depth δ of THz SPP field in air the process of SPP excitation on a bare metal surface is rather embarrassing, which results in very low transformation efficiency (from hundreds to thousandths of a percent) of bulk radiation into THz SPP.

To transform bulk radiation into SPP one has to match their phase velocities and the tangential components of the wave vectors. In the visible range these conditions could be met using a diffraction grating formed on a metal surface or a prism made of a material optically denser than the environment (the attenuated total reflection (ATR) method). But in the IR and far IR ranges, the ATR method works badly as an introduction of a prism into the SPP field changes the guiding structure (and the SPP characteristics, accordingly) to a very large extent, radically increasing SPP radiation losses and overlapping access to the surface under study. That is why the preferred opportunity to excite THz SPP by bulk radiation is its diffraction on an object disposed on the surface or in its vicinity.

The prime experiments on THz SPP excitation were performed about 30 years ago with a silicon prism as a coupling element and a "whisky" laser generating at λ=118 μm[18,19]. Note, that in this case the prism was used not to realize the ATR method but to employ the aperture method of SPP excitation (the laser radiation was directed through the prism onto the prism edge and diffracted on it)[20]. Several unpredicted and astonishing facts were established: 1) THz SPP propagation length L was found to be from one to two orders smaller as compared with the value of L calculated using the Drude model for the dielectric function of the metal; 2) the efficiency

---

[18] Begley D.L., Alexander R.W., Ward C.A., Miller R., and Bell R.J. Propagation distances of surface electromagnetic waves in the far infrared // Surface Science, 1979, v.81, p.245-251.

[19] Koteles E.S., McNeill W.H. Far infrared surface plasmon propagation // Int. J. Infr. & Millim. Waves, 1981, v.2(2), p.361-371.

[20] Zhizhin G.N., Moskalova M.A., Shomina E.V., and Yakovlev V.A. Selective absorption of surface EM waves, propagating along metal covered by a dielectric film // JETP Lett. (USA), 1976, v.24(4), p.196–199.

of the radiation transformation into SPP turned to be as low as hundredths of a percent if not less; 3) this transformation was accompanied by production of strong parasitic beams of diffraction origin propagating away from the surface or along it, their fields thus superimposed on the SPP field. Later on, similar experiments were done with gratings (of various profiles)[21] and screen edges[22] used for coupling incident radiation and THz SPP via diffraction.

Unexpectedly small values of L for THz SPP have been interpreted in many ways, but to our mind the difference in the dielectric function of the metal surface and its crystal state on the one hand and enormous radiation losses of SPP on inhomogeneities of the bare metal surface on the other seems to be the most probable explanation for the effect.

The problem of tiny transformation efficiency took a lot of effort to bridge it over. First it was suggested to cover the metal surface with a dielectric layer, which resulted in dramatic redistribution of SPP field from air into the metal and its more pronounced adhesion to the surface[23]. Later on a good deal of labor was spent on experiments aimed at searching for some specific profile of a diffractional grating ensuring the maximal excitation efficiency of THz SPP[24]. Finally it was established that the best efficiency (tens of percent) for THz SPP excitation by bulk radiation is reached when a diffractional grating (with sin profile and groove depth of about $\lambda/10$) covered with a dielectric layer is used[25].

But diffractional gratings have such important disadvantages as non-mobility and exerting damage to the specimen, what is often unacceptable. That is why in addition to the aperture method for THz SPP excitation the waveguide method was elaborated, which implies positioning an object (say a prism) with a plane metallized facet paral-

[21] Schlesinger Z. and Sievers A.J. IR surface-plasmon attenuation coefficients for Ge-coated *Ag* and *Au* metals // Phys. Rev.(B), 1982, v.26(12), p.6444-6454.
[22] Zhizhin G.N., Alieva E.V., Kuzik L.A. et al. Free-electron laser for infrared SEW characterization of surfaces of conducting and dielectric solids and nm films on them // Appl. Phys.(A), 1998, v.67, p.667-673.
[23] Seymour R.J., Krupczak J.J., Stegeman G.I. High efficiency coupling to the overcoated surface plasmon mode in the far infrared // Appl. Phys. Lett., 1984, v.44(4), p.373-375.
[24] Martl M., Darmo J., Unterrainer K., and Gornik E. Excitation of terahertz surface plasmon polaritons on etched groove gratings // JOSA(B), 2009, v.26(3), p.554-558.
[25] Cleary J.W., Medhi G., Peale R.E., and Buchwald W.R. Long-wave infrared surface plasmon grating coupler // Appl. Opt., 2010, v.49(16), p.3102-3110.

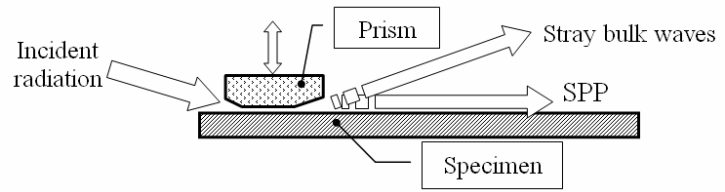

Fig.1. Schematic of the waveguide method for THz SPP excitation.

lel to the specimen surface thus forming a shallow waveguide[26] (Fig. 1). Being directed at the entry slit of the waveguide the incident radiation excites modes of TM type (the single-mode regime – preferable). Diffracting on the prism exit edge the modes convert into SPP with a number of percent parts efficiency, which (similarly to the grating excitation method) is proportional to the dielectric coverage thickness.

II.2. ***Suppression of THz SPP diffraction satellites***

The diffraction mechanism of the incident radiation conversion into the surface wave is predominating for all the known methods of THz SPP excitation (aperture, prism, grating, etc.). Therefore, their excitation by a laser beam (which is preferred in SPP absorption spectroscopy) is accompanied by the generation of intense parasitic (stray) bulk waves of a diffraction nature (diffraction satellites), which may spatially coincide with THz SPP[27]. There are several known methods for suppressing the diffraction interference:

(i) arrangement of a nontransparent screen (oriented perpendicularly to the SPP track) over the surface[28]. However, this approach results in that now SPP (rather than the incident bulk wave) exhibits diffraction on the screen edge, which leads to the Lloyd's interference of rays emitted from the edge and the appearance of its image in the mirror specimen surface;

(ii) arrangement of both elements of the transformation (from bulk radiation into SPP and vice versa) on separate specimen surfaces conjugated by a rounded edge[19].

[26] Jeon T.-I., Grischkowsky D. THz Zenneck surface wave (THz surface plasmon) propagation on a metal sheet // Appl. Phys. Lett., 2006, v.88, 061113.

[27] Gong M., Jeon T.-I., and Grischkowsky D. THz surface wave collapse on coated metal surfaces // Opt. Express, 2009, v.17(19), p.17088-17101.

[28] Silin V.I., Voronov S.A., Yakovlev V.A., and Zhizhin G.N. IR surface plasmon (polariton) phase spectroscopy // Int. J. Infr. & Millim. Waves, 1989, v.10(1), p.101-120.

In this case, the photo detector should be moved to a substantial distance from the edge in order to reduce significantly a contribution of the diffracted radiation to the photocurrent;

(iii) formation of a cylindrical trench into the surface, which is oriented perpendicularly to the SPP track, and the arrangement of a nontransparent screen over the trench bottom, with the screen edge fixed in the trench on a level below the surface[26]. This solution has much in common with method (i), including all its drawbacks;

(iv) formation of a conical trench (geodesic prism) on the surface, which axis is oriented perpendicularly to the SPP track and whose generatrix obeys a linear law[29]. This trench drives the SPP to deviate from the initial propagation direction, but does not act upon the diffracted radiation, which ensures the spatial separation of the SPP and the parasitic bulk waves.

As the last-named method is not obvious let us consider it in detail. Assume that we have the task of determining the terms when a geodesic prism deflects a collimated THz SPP beam without distorting its wave front and deriving a formula for calculating the angle of SPP deflection from its initial direction of propagation. Suppose a collinear beam of a width w of SPP rays characterized by a complex index of refraction $\kappa=\kappa'+i\cdot\kappa''$ propagates along a plane surface. Let an inhomogeneity in the form of a trench be created in the surface normal to the initial wave vector of the SPP (Fig. 2). We shall prove that if the trench has the form of a right cone with its axis lying in the specimen surface, such a trench ensures that SPP optical path depends linearly on the coordinate x, i.e. such a trench is a geodesic prism capable of turning the SPP wave front through an angle γ.

Let us estimate ΔS_o, the difference in the geometrical paths of the extreme rays of the SPP beam incident on the trench, introducing the following notations: R_o is the radius of the "cone" base, R is the current radius of the trench surface, which depends on the coordinate x, H is the "height" of the "cone" (equal to the beam width w). To

[29] Bogomolov G.D., Zhizhin G.N., Nikitin A.K., and Knyazev B.A. Geodesic elements to control terahertz surface plasmons // Nuclear Instruments and Methods in Physics Research (A), 2009, v.603(1/2), p.52-55.

determine ΔS_o we will single out on the specimen surface a box enveloping the trench having dimensions $2R_o \times H$. The geometrical path S_o of an arbitrary SPP ray inside the inhomogeneity depends upon the coordinate x as follows: $S_o(x)=2(R_o-R)+\pi \cdot R = R_o \cdot [(x/H) \cdot (2-\pi)+\pi]$, where it is taken into account that $R=(R_o/H) \cdot (H-x)$. Hence, the value of S_o depends linearly on x.

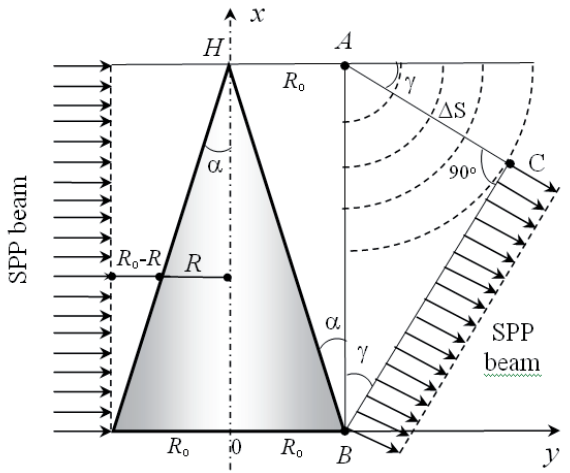

Fig. 2. SPP beam with plane wave front overcoming the inhomogeneity with dimensions $2R_o \times H$ containing a conical trench.

Furthermore, the geometrical path difference ΔS_o for the extreme rays of the beam (characterized by the coordinates $x=0$ and H) is given by $\Delta S_o=S_o(0)-S_o(H)=R_o(\pi-2)$, while the optical path difference of these rays is given by $\Delta S=\Delta S_o \cdot \kappa'=R_o(\pi-2) \cdot \kappa'$. Therewith, the ray with coordinate $x=H$ will cover the box faster than the ray with the coordinate $x=0$. The time interval is $\Delta t=\Delta S/\vartheta=[R_o \cdot (\pi-2) \cdot \kappa']/(C/\kappa')$; where ϑ is the phase velocity of SPP, C is the speed of light in vacuum. That is why the point A becomes a source of secondary waves with circular wave fronts by Δt earlier as compared with the point B. During the time interval Δt, the secondary waves will cover the distance $AC=\vartheta \cdot \Delta t=\Delta S=R_o \cdot (\pi-2) \cdot \kappa'$. Finally, from the rectangular triangle ABC one can find that $sin(\gamma)=AC/H=[R_o \cdot (\pi-2) \cdot \kappa']/H=tan(\alpha) \cdot (\pi-2) \cdot \kappa'$. Thus, the final formula

for calculating γ, the angle of SPP beam deflection by a conical trench, looks as follows:

$$\gamma = arcsin[tan(\alpha)\cdot(\pi\text{-}2)\cdot\kappa'']. \quad (1)$$

Note that the angle γ depends upon $tan(\alpha)$, i.e. upon the ratio of the trench radius R_o to the beam width w. Therefore, the method for deflecting a SPP beam with a conical trench can be used only under the condition that the SPP propagation length L exceeds well the trench radius R_o. Otherwise, the SPP will dissipate on their way across the trench. This condition is met for SPP in the THz range as at these frequencies L reaches dozens of centimeters and even more.

The dependence of $S_o(x)$ is not linear if the axis of the cone does not lie in the specimen surface, which results in divergence of the SPP rays that have covered the trench. This leads to a distortion in the wave front, which is unacceptable for beam deflectors. But the requirement on the cone top location in the beam span is not a prerequisite; formula (1) is also valid for a case when the cone top is out of (or inside) the beam margins. And one more remark in conclusion of this paragraph: to reduce radiation losses one has to smooth the trench edges with a radius of rounding r satisfying the condition $r>>\lambda$.

By the example of SPP geodesic prism operation, let us calculate the value of the angle α between the moving line of the conical trench and its axis to deflect a collimated SPP beam excited with monochromatic radiation (λ=110 μm) on a plane aluminum surface bordering air to the angle γ equal to 30^o. In this case, the real part of the SPP refractive index is κ''=1.0005 and the SPP propagation length L calculated using the Drude model for aluminum dielectric permittivity equals 685 cm, which meets the condition $L>>R_o$ with a safety margin. Substituting values for κ'' and γ in Eq. (1), we get $\alpha\approx24^o40'$.

Note, that a system of two conjugated geodesic prisms whose axes coincide and lie in the specimen surface can play the role of SPP beam splitter (Fig. 3). The condition of coincidence of the prisms tops is not binding; location of the tops in the trench axis is quite sufficient. It is evident that the splitting angle γ between the new diverg-

ing SPP beams equals the sum of the deflection angles γ_1 and γ_2 introduced by each of the prisms:

$$\gamma = \gamma_1 + \gamma_2 = arcsin[tan(\alpha_1)\cdot(\pi - 2)\cdot\kappa'] + arcsin[tan(\alpha_2)\cdot(\pi - 2)\cdot\kappa'], \qquad (2)$$

where α_1 and α_2 are the angles between the moving lines of the prisms and their common axis, respectively. Such SPP beam splitters can be utilized in SPP interferometers, sensors, and communication devices.

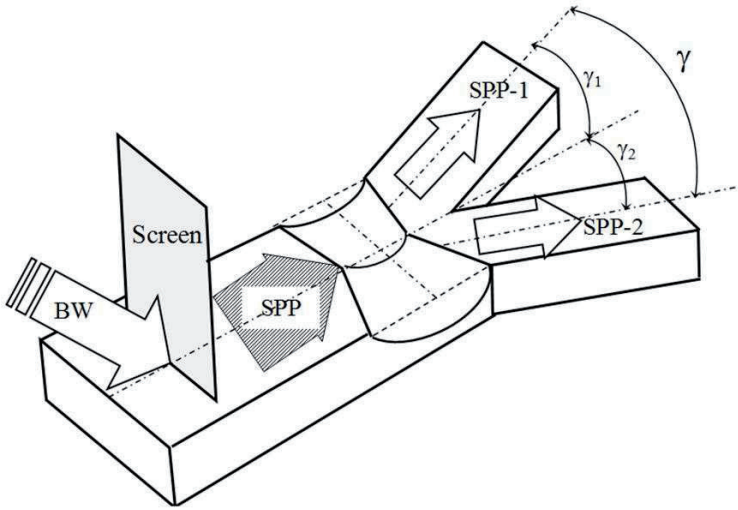

Fig. 3. Geodesic SPP beam splitter: BW – incident bulk wave; SPP - initial SPP beam; SPP-1 and SPP-2 - new SPP beams.

II.3. *Method for detecting diffraction satellites of THz SPP*

Yet, in spite of all these tricks, it turned out to be impossible to suppress thoroughly the stray bulk waves generated in the process of THz SPP excitation by light. Moreover identification of THz SPP themselves is not as simple as it is the middle IR. In the latter case SPP are identified employing the following signs:

(i) vanishing of the signal from a photodetector (monitoring SPP) when the polarization is switched from *p*- to *s*-type;

(ii) exponential decay of the intensity with increasing the distance from the input element;

(iii) exponential decay of the field intensity on going away from the surface;

(iv) temporal sharp decrease of the radiation intensity detected at the specimen edge after condensation of breath expired moisture on the surface.

However, all these signs are less pronounced in the THz range. In particular, diffraction at the screen (prism) edge is also sensitive to a change in the polarization of radiation. The exponential decay of the THz SPP is difficult to reveal on a 10–20 cm long specimen. Measurements of the exponential decay of THz SPP intensity along the normal to the surface are possible only in the absence of diffraction satellites. Finally, the change of SPP intensity response to the condensate formation is masked by the absorption of THz radiation by the expired water vapor.

Thus, in view of the fact that it is practically impossible to get rid of the diffraction satellites and that they hinder the identification and exploring of THz SPP the task of detecting and identifying diffraction bulk waves in the THz SPP field is of considerable importance.

Such method was suggested in the paper[30]. The backbone of the proposed method is in measuring the SPP intensity change upon sequential application of the same local thin film coating at various sites onto the SPP track.

First let's demonstrate that the application of such a coating in any two regions of the track of SPP not accompanied by diffracted radiation beams must lead to identical changes in the intensity of SPP detected at any same point of the track (e.g., at the specimen edge).

Evidently, the application of a local coating element of length a on the surface would provide additional SPP damping because of (i) an increase in the Joule heat losses as a result of the SP field redistribution from air into the metal and (ii) the appearance of additional radiative losses as a result of the SPP diffraction on edges of the coating element. Let's take both these types of losses into account by introducing absorption coefficient β.

Suppose the coating element is applied in position 1, where its frontal edge has a coordinate x=0, and a distance from the right-hand edge of the element to the right-

[30] Gerasimov V.V., Knyazev B.A., Nikitin A.K., Nikitin V.V. Method for identifying diffraction satellites of surface plasmons in terahertz frequency range // Techn. Phys. Lett., 2010, v.36 (11), p.1016–1019.

hand sample end (where the photodetector is situated) is $x=b$ (Fig.4). If the initial SPP field intensity at point $x=0$ is I_0, then the attenuated intensity is $\beta \cdot J_0$ and the intensity measured by the detector will be

$$I_1 = I_0 \cdot \beta \cdot exp(-\alpha \cdot b), \quad (3)$$

where α is the SPP absorption coefficient on the sample surface free of the coating.

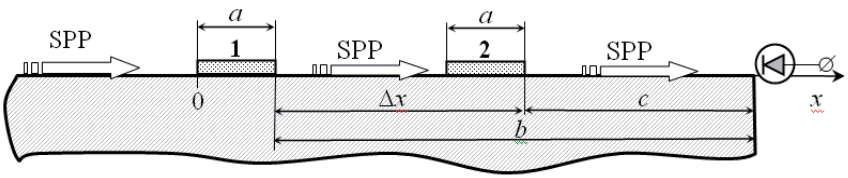

Fig. 4. Arrangement of a local coating element of length a on the surface guiding THz SPP.

After displacement of the coating by a distance of Δx to position 2, the SPP intensity measured by the photodetector will be

$$I_2 = I_0 \cdot \beta \cdot exp(-\alpha \cdot \Delta x) \cdot exp(-\alpha \cdot c) = I_0 \cdot \beta \cdot exp[-\alpha \cdot (\Delta x + c)] = I_0 \cdot \beta \cdot exp(-\alpha \cdot b), \quad (4)$$

where c is the distance traveled by the SPP from the element in position 2 to the detector. As one can see, $I_1=I_2$, which implies that the SPP intensity in the absence of diffraction satellites decreases by the same amount, irrespectively of the coating position on the SPP track.

With respect to the direction of propagation, the diffraction satellites of SPP can be subdivided into three groups, which include the wave propagating strictly parallel to the surface and those having a wave vector component directed either toward the surface or outward. For the satellites directed outward, the photodetector can be protected as described in [19]. Satellites directed at a small angle relative to the surface or parallel to it can generate parasitic signal in the detector. The method developed is aimed at detecting THz SP satellites of this kind.

Let us assume that SPP are accompanied by satellite beams directed toward the surface. Then, the application of a coating element on various parts of the SPP track will result in the detection of different signals. Indeed, since the satellites will reflect from the coating when it is in one position and from the sample surface when the

element is in the other position, the photodetector response in the two cases will be different.

In their turn satellites traveling strictly parallel to the surface can be identified as follows. As is known[21], the application of an extended coating with a thickness on the order of λ/10 decreases THz SPP propagation length L by two orders of magnitude and makes $L \approx 10\lambda$. Therefore, if the SPP are not accompanied by volume satellites propagating along the surface, then the application of a blackened plate made of a transparent material (e.g. paper) will lead to vanishing of the signal. In contrast, if these satellites are present, the signal will only decrease to a certain level, which can be either considered as a constant background or compensated by adjusting the optical system.

II.4. *THz SPP spectrometers of absorption type*

The SPP technique enables scientists to obtain enhanced absorption spectra of surfaces and their transition layers as excitation of SPP is accompanied by a resonant amplification of the incident wave field lifting it up to two or even three orders of magnitude. SPP-spectroscopy falls in the category of non-destructive methods of surface characterization used not only in vacuum but under natural conditions as well.

The method foundations were laid dawn in 1973, when American scientists managed to measure SPP propagation length L in infrared directly using a CO_2-laser and the two-prism technique for the SPP excitation and detection[31]. The method turned to be rather simple for realization, reliable and very sensitive; it gained wide recognition and was mastered in Russia as well [20].

The method of absorption SPP-spectroscopy implies determination of the surface wave propagation length L in a definite frequency range. To implement the method in case of a tunable source of radiation one has to measure the field intensity I_1 and I_2 at (at least) two successive points of the SPP track characterized by coordinates x_1 and x_2. Then the value of L can be computed by the formula:

[31] Schoenwald J., Burstein E., and Elson J.M. Propagation of surface polaritons over macroscopic distances at optical frequencies // Solid State Comm., 1973, v.12 (3), p.185-189.

$$L = \frac{x_2 - x_1}{ln(I_1/I_2)}. \qquad (5)$$

Measurements of L should be carried out for the bare metal surface bringing the value of L_o, as well as for the surface containing the film under study bringing the value of L_f. Thus decrease in L at a definite frequency ν due to the film presence will be $\Delta L = L_o - L_f$. The dependence $\Delta L(\nu)$ obtained for a number of frequencies ν attributed to the range will represent itself the enhanced absorption spectrum of the film in this range.

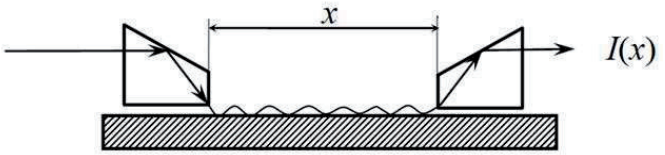

Fig. 5. The scheme of the two-prism method for IR SPP propagation length L measurements.

The scheme of the set-up realizing the method is sketched in Fig.5. As an example the aluminum oxide spectrum obtained by the SPP-spectroscopy method in the middle IR is given in Fig.6. The dependence of the SPP normalized intensity I on wavelength λ was measured three times for the fixed distance x=60 mm run by the wave. One can see a well-pronounced absorption band of the oxide layer (3 *nm* thick) in the neighborhoods of λ=10.6 μ*m*[32].

Note that while performing SPP-spectroscopy an increase of measurements sensitivity takes place not only due to the field amplification in the space near the surface, but because of the enlargement of radiation-sample interaction distance as well. That is way the SPP-spectroscopy makes it possible to investigate monolayer (actually even submonolayer) films on solid surfaces.

Up to the preset SPP-spectroscopy technique was practiced mainly in relatively narrow spectral regions adjacent to more intense lines of generation of *CO*, CO_2-

[32] Alieva E.V., Beitel G., Kuzik L.A. et al. Linear and nonlinear FEL-SEW spectroscopic characterization of nanometer-thick films // Appl. Spectroscopy, 1997, v.51 (4), p.584–591.

lasers [20], as well as methanol vapor lasers[33]. As soon as FELs were built scientists could study another important feature of SPP – the dispersion in broad areas of optical frequencies ranging from plasma (~50000 cm^{-1}) to THz frequencies[34].

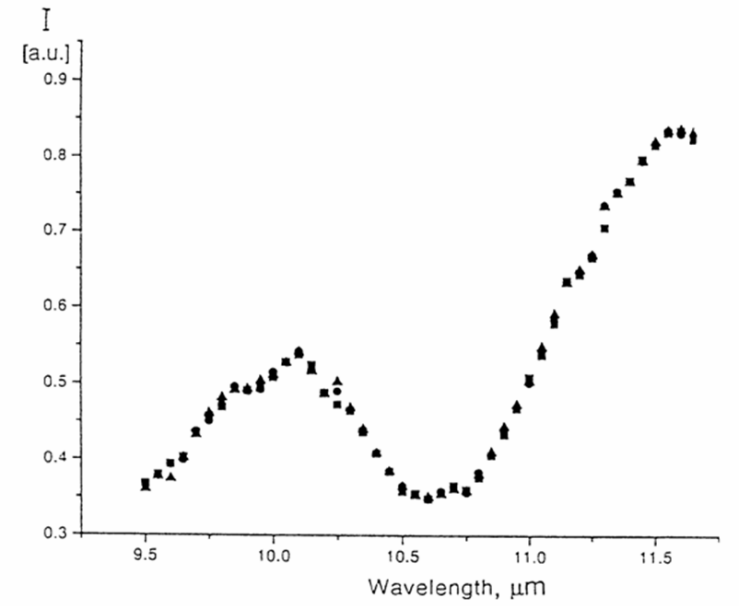

Fig. 6. The SPP transmission spectrum of the natural aluminum oxide film obtained by the two-prism method at FELIX in the Netherlands[32].

Thus, main problems facing absorption SPP-spectroscopy in the THz range as compared with the middle IR are: 1) presence of diffraction bulk satellites overlapping with the field of SPP and 2) small excitation efficiency of SPP by bulk radiation. But both these difficulties are not impassable: the satellites could be shielded and detected, while SPP intensity could be increased whether via up-grading SPP excitation efficiency by covering the specimen surface with a dielectric layer or via employing such powerful sources as FELs or synchrotrons.

[33] Schlesinger Z., Webb B.C., and Sievers A.J. Attenuation and coupling of far-infrared surface plasmons // Sol. St. Comm., 1981, v.39(10), p.1035-1039.

[34] Alieva E.V., Kuzik L.A., Yakovlev V.A., Zhizhin G.N. Study of crystals in medium and long-wavelength IR ranges by surface electromagnetic wave spectroscopy // Phys. Solid State, 1998, v.40(2), p.213-216.

II.4.1. ***Dynamic spectrometers***

Devices of this type can be used in case when it is necessary to investigate a limited number of samples with relatively stable layers under study employing (continues-wave) CW or quasi-CW lasers, like FELs.

In theory the two-prism scheme used for measuring L in IR may be applied at THz frequencies as well and first experiments on THz SPP measurements were performed employing the scheme [19]. As SPP excitation in this scheme takes place exceptionally due the incident radiation diffraction on the prisms edges the prisms were replaced afterwards[32] with more handy plane screens brought to the specimen surface to a distance of tens of λ. But SPP excitation efficiency for screens proved to be very low that implied the signal acquisition with a cooled detector.

Finally investigators came to the opinion that diffractional gratings covered with a dielectric layer are the most efficient transducers of THz bulk waves into SPP [35, 23, 36]. But grating couplers, as noted above, are non-mobile and exert damage to the specimen. This is unacceptable in case of a unique specimen. The harmless waveguide method elaborated by Professor Daniel R. Grischkowsky and coworkers [26] is more suitable for measurements with varying SPP propagation distance.

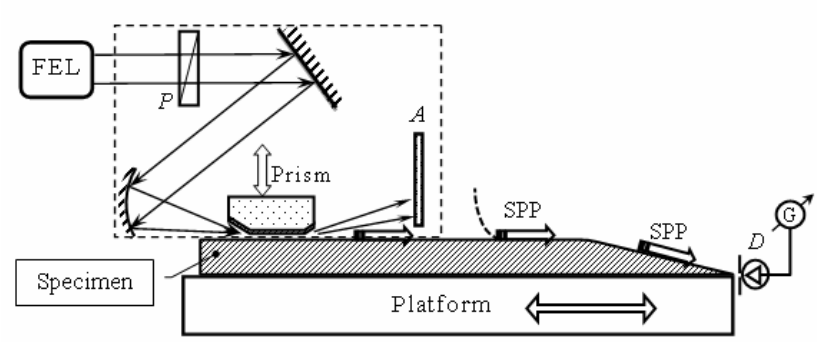

Fig. 7. Schematic of a dynamic THz SPP spectrometer able of varying the distance run by SPP by moving the specimen relative to the fixed input prism.

[35] Seymour R.J., Koteles E.S., and Stegeman G.I. Infrared surface plasmon coupling with overcoated gratings // Appl. Phys. Lett., 1982, v.41(11), p.1013-1015.
[36] Nazarov M., Shkurinov A., Garet F., Armand D., and Coutaz J.-L. Surface plasmon THz waves on gratings // C. R. Physique, 2008, v.9(2), p.232-247.

Fig.7 sketches the device we used in the experiments. It employs the reverse configuration of the specimen, i.e. an element converting an incident radiation into SPP is placed on the long plane part of the specimen surface under study, while a detector is disposed at the edge of its short part. Collimated monochromatic THz radiation produced by FEL passes through a revolving polarizer *P* and on reflection from the plane and cylindrical mirrors is focused at the entry mouth of the input prism. TM-modes are exited by the radiation in the gap between the prism basement and the specimen surface. On the outlet prism mouth the modes diffract and partially convert into SPP. The diffracted bulk waves are blocked by absorber *A*, while the SPP slip under it. Detector *D*, fixed at the edge of the specimen and provided with an aperture, indicates the SPP arrival. To change the distance run by the SPP the specimen may be installed on a computer-controlled horizontally moving platform.

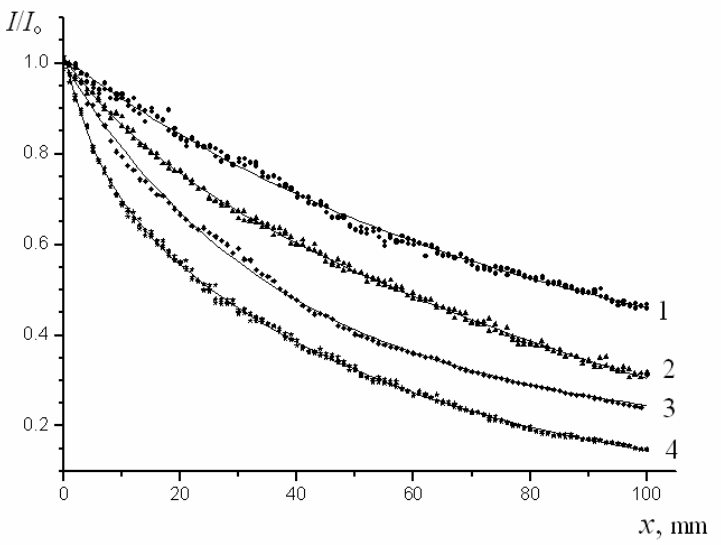

Fig. 8. Experimental dependences of normalized SPP intensity I/I_o (λ=110 μm) on the SPP run distance *x* measured for *Al* surface covered with a *Ge* layer of thickness *d*: (1) *d* =0; (2) 0.5; (3) 1.0, and (4) 2.0 μm.

A setup implementing the scheme presented in Fig.7 was built at the Budker Institute of Nuclear Physics (Novosibirsk, Russia), where the NovoFEL generating THz

radiation is functioning[37]. The setup was employed for study of THz SPP excited on gold, copper and aluminum. As an illustration of THz SPP sensibility to presence of a dielectric layer on the guiding surface experimental dependences of normalized SPP (λ=110 μm) intensity I/I_o on the run distance x measured for aluminum covered with germanium layer of different thickness d are displayed in Fig.8[38]. One can see that SPP preserve their sensibility to subwavelength overlayers at THz frequencies and that *Ge* layers of thickness less than $\lambda/100$ may be surely detected.

Other designs of devices for measuring THz SPP propagation length L have been elaborated and described elsewhere [39, 40].

II.4.2. ***Static spectrometers***

Static SPP spectrometers are useful when fast processes going on the surface are investigated. In this case, the SPP propagation length L has to be determined within the time interval comparable with one laser pulse duration.

We have developed two designs of static devices for determining THz SPP propagation length L able to obtain absorption spectra of thin films provided a tunable monochromatic source is employed.

The first device[41] is of ATR type which is used in the THz spectral range rather seldom. As it was noted above the ATR prism being introduced in the SPP field in order to excite the SPP effectively distorts the field to a large extent. But in case of a powerful source the distance h, spacing the prism from the specimen surface containing a layer under study, may be larger than the SPP field penetration depths δ into air and thus the prism influences the value of L negligibly. The novel part in the device is the ATR element itself: it is made of a transparent material in the form of a long

[37] Knyazev B.A., Kulipanov G.N., and Vinokurov N.A. Novosibirsk terahertz free electron laser: instrumentation development and experimental achievements // Measurement Science and Technology, 2010, v.21, 054017.

[38] Zhizhin G.N., Nikitin A.K., Bogomolov G.D. et al. Absorption of surface plasmons in a metal-cladding layer-air structure in the THz frequency range // Optics and Spectroscopy, 2006, v.100(5), p.734-738.

[39] Zhizhin G.N., Mustafina O.M., Nikitin A.K. A device for measuring IR SPP propagation length // Patent of Russia on invention, 2010. - No.2380664.

[40] Nikitin A.K., Zhizhin G.N., Mustafina O.M., Rijova T.A. A device for determining IR SPP absorption coefficient // Patent of Russia on invention, 2010. – No. 2380665.

[41] Nikitin A.K., Zhizhin G.N., Bogomolov G.D. et al. A device for obtaining absorption spectra of thin films in the THz spectral range // Patent of Russia on invention, 2009. - No.2345351.

plane-parallel plate 2 provided with a tapered end surface and its base extending along the SPP track (Fig. 9). In this way the optical coupling between the specimen

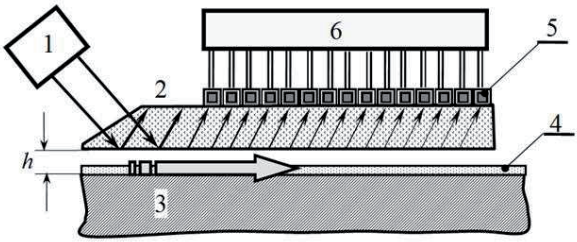

Fig. 9. Schematic of the static THz SPP spectrometer of ATR type: 1 – source of monochromatic radiation; 2 – elongated ATR prism; 3 – metal specimen; 4 – layer under study; 5 – photo detector array; 6 – computer.

surface and the ATR prism does not die out and the SPP radiates into the prism at each point of its track. Proportional to intensity of the SPP at any point of the track the reradiated light is registered by photo detector array 5, which produces electrical signals executed by computer 6 to calculate the value of L. Similar measurements for the bare metal surface at other frequencies ν of radiation in the spectral region of interest bringing the dependence of $L_o(\nu)$ should be performed. On the second stage the dependence of $L_f(\nu)$ for the surface with the layer under are to be obtained. The difference $\Delta L(\nu)=L_o(\nu)-L_f(\nu)$ will represent the desired absorption spectra of the layer.

The second device employs splitting of the initial THz SPP beam into two new ones which run different distances along noncoinciding tracks on the specimen surface[42]. The scheme of the device implementing this idea is presented in Fig.10. Beam1 of bulk monochromatic radiation is converted into a beam of SPP by element 2. On encountering beam splitter 3 (e.g. a corner mirror) the SPP beam is divided into two new SPP beams equal in power and propagating in opposite directions. Having run different distances the beams are focused by plane lenses 4 (e.g. geodesic ones) onto corresponding detectors 5, which produce electrical signals proportional to the

[42] Zhizhin G.N., Nikitin A.K., Nikitin V.V., and Chudinova G.K. Method for determining IR surface electromagnetic wave absorption coefficient for the one radiation pulse duration // Patent of Russia on invention, 2010. - No.2400714.

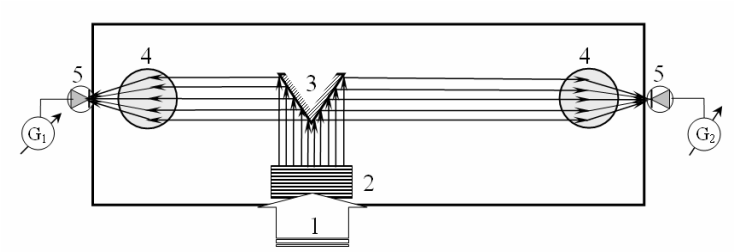

Fig. 10. Schematic of the static double-beam THz SPP spectrometer (top view):
1 – beam of monochromatic radiation; 2 – SPP coupling element;
3 – beam splitter; 4 – planar lenses; 5 – photo detectors.

intensity of the relevant SPP beam. On registering the signals one can calculate the value of L provided the distances run by the oppositely propagating beams are known. The same measurements are supposed to be performed for other frequencies of radiation in the working range.

II.5. *Amplitude THz SPP refractometry*

Dielectric permittivity is of great importance for many practical applications of metals, namely for calculations of the radiative balance of spaceships, remote radiometry, modeling special mirrors and protecting coverings, etc. The need for far IR data is also provoked by the increasing application of the THz waves to communication problems.

However, no metal permittivity has been measured up to now as none of the applicable optical refractometry methods (absorption reflectometry, ellipsometry, Fourier-spectroscopy and others) is able to measure it in the far IR range, due to high reflectivity of metals. Handbooks of optical constants (see, e.g. [3]) present data restricted by the long wavelength limit of 25 μm for only twelve metals.

Here we present the possibility for determining the optical constants (or dielectric function) of real metal surfaces at THz frequencies by measuring the SPP propagation length L and the SPP field penetration depth δ in air.

It is well known that solving the dispersion equation for SPP in a given guiding structure, one can determine two its parameters provided the complex refractive in-

dex $\kappa=\kappa'+i\cdot\kappa''$ of the surface wave is measured. Specifically, in case of a two-layer structure composed of a plane metal surface and adjacent air, the equation having the following form:

$$\kappa=\sqrt{\frac{\varepsilon_1\cdot\varepsilon_2}{\varepsilon_1+\varepsilon_2}} \tag{6}$$

(here $\varepsilon_1=\varepsilon_1^{'}+i\cdot\varepsilon_1^{''}$ and $\varepsilon_2=\varepsilon_2^{'}+i\cdot\varepsilon_2^{''}$ are the dielectric functions of the metal and that of air, accordingly) may be resolved relative to $\varepsilon_1^{'}$ and $\varepsilon_1^{''}$.

So, the only problem in the THz SPP refractometry of real conducting surfaces is the determination of κ, consisting of κ' and κ''.

One can determine κ'' by measuring the value of L with the procedures described above and solving the equation $L=(2k_o\cdot\kappa'')^{-1}$ relative to κ''.

As for the value of κ' specifying the SPP phase velocity it seems, at first sight, that it can be determined by interferometric measurements and no other. Nevertheless recently an amplitude approach for κ' determination was developed and tested [43]. The point is that on the one hand the value of δ depends on κ, while on the other hand it can be easily measured at THz frequencies with a photo detector array or a single moveable detector. The dependence of δ on κ is as follows[4]:

$$\delta=\left[k_o\cdot Re\left(\sqrt{\kappa^2-\varepsilon_2}\right)\right]^{-1}. \tag{7}$$

Evidently, the quantity of κ' being a part of κ can be expressed via preliminary experimentally determined quantities of κ'' (or L) and δ. The execution of eq.(7) relative to κ' is presented in Appendix 1 and has the following form:

$$\kappa'=\frac{k_o^2\delta^2\kappa''\varepsilon_2''}{2\cdot\left[1+k_o^2\delta^2\cdot\left(\kappa''\right)^2\right]}+\sqrt{\frac{1}{1+k_o^2\delta^2\cdot\left(\kappa''\right)^2}}\times\left[\frac{1}{k_o^2\delta^2}+\left(\kappa''\right)^2+\varepsilon_2'-\frac{k_o^2\delta^2\cdot\left(\varepsilon_2''\right)^2}{4\cdot\left[1+k_o^2\delta^2\cdot\left(\kappa''\right)^2\right]}\right]. \tag{8}$$

Note that formula (8) is reduced to formula (10) in [44], provided $\varepsilon_2''=0$.

[43] Gerasimov V.V., Knyazev B.A., Nikitin A.K., and Zhizhin G.N. A way to determine the permittivity of metallized surfaces at THz frequencies // Appl. Phys. Lett., 2011, v.98, 171912.

[44] Nikitin A.K., Khitrov O.V., Kyrianov A.P., Knyazev B.A., and Zhizhin G.N. Surface plasmon dispersive spectroscopy of thin films at THz frequencies // Proc. SPIE, 2010, v.7376, 7376 0U.

Fig.7 sketches the device used in the experiments testing the elaborated technique, except for the specimen had plane top surface with no backfall and the detector *D* was able to move in the plane of incidence in order to be able of measuring the SPP field distribution in air.

The specimen was a firm aluminum plate (40 mm wide and 250 mm long) with optically polished top surface covered with a thermally evaporated 1 μm thick gold film. The input element was made of glass in the form of prism with the right-angle box cross-section, the 40×40 mm^2 top base and the 20×40 mm^2 bottom base; the cut angles of the bottom base were 20^o and 8^o for the entry and exit mouths, accordingly. A wadding sheet disposed at 35 mm from the prism and raised 3 mm over the sample was used as absorber *A*. The intensity of the SPP field was measured by a Golay cell with optical sensitivity of 10^5 V/W. The experiments were performed at the Novosibirsk FEL (NovoFEL) generating within the spectral ranges of 120-240 μm and 40-70 μm a continuous stream of 100-ps pulses with a repetition rate of 5.6 MHz, the average power of the radiation at the user stations being around ten watts [37].

The measurements were performed in the air atmosphere with the absorption coefficient $\alpha=2k_ok_2=0.173$ m^{-1} (here k_2 is the absorption index of air) at $\lambda=130$ μm. To make sure that we dealt namely with SPP the following tests were used:

1) polarization change from *p*- to *s*-type led to disappearance of the signal produced by the detector;

2) measured decay of the wave field intensity both along the surface and the normal to it proved to be exponential;

3) an approximate permanence of the photo signal as a standard paper strip put on the surface and crossing the track at the right angle was moved along the track [30].

Figs.11 and 12 present results of the measurements. In the graphs, the vertical axes correspond to normalized signals U/U_{max} produced by the detector, while the distance *x* (run by the SPP) and the span *z* from the sample surface refer to the *x*-coordinates, respectively. The exponential character of the decay of the dependences is obvious, though some interference oscillations could be distinguished in both graphs if one connects the experimental points without the approximations. It means

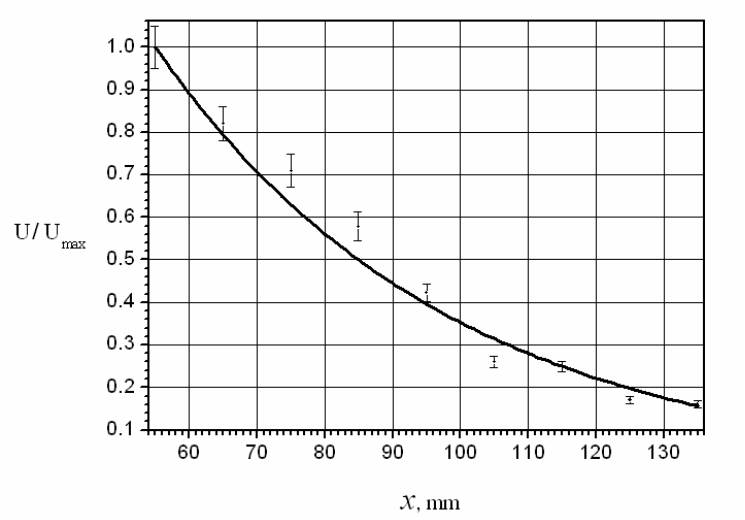

Fig. 11. Measured dependence of the normalized SPP field intensity on the distance *x* run by the wave along the gold-air interface.

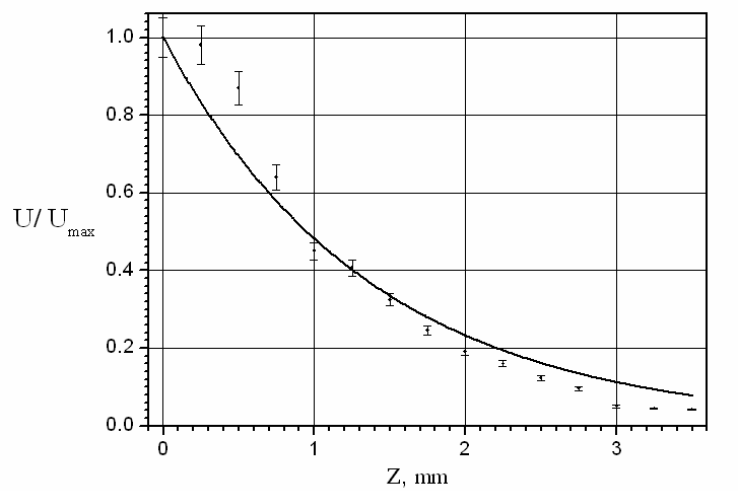

Fig. 12. Profile of the normalized SPP field intensity along the *z* axes, normal to the *Au*-air interface, measured at the distance of 13.5 cm from the input element.

that absorber *A* failed to block all the diffracted bulk waves and that some extra measures should be undertaken to clear the diffractional noise from the SPP field.

According to the measured dependences of the SPP field intensity on *x* and *z*, it decreases by a factor of 1/*e* at the distance *L*=38.4 mm along the SPP track and at the distance δ=1.3 mm along the normal to it. Substituting the magnitude of *L* in $L=(2k_o\cdot\kappa'')^{-1}$, we calculated $\kappa''=2.7\cdot10^{-4}$. After that we put the values of κ″ and δ in eq.(8) and computed the corresponding value of κ′=1.000657. Taking into account the value for α in air and the fact that the refractive index of air n_2 at THz frequencies equals 1.0002726, we found the air permittivity $\varepsilon_2 = \varepsilon_2^{'} + i\cdot\varepsilon_2^{''} = (n_2+i\cdot k_2)^2 = 1.000545 + i\cdot0.0000036$. Finally, substituting the values of κ′, κ″ and ε_2 in eq.(6) and solving it relative to ε_1, we determined the permittivity of the evaporated gold surface $\varepsilon_1 = - 877 + i\cdot610$.

To check the validity of the procedure for ε_1-estimation, we compared values of the relation δ/*L* composed of the experimental results and those calculated using the approximate formulae for δ and *L* given in[45]. The first value equals 0.034 and the second – 0.025, that is 25% mismatch.

Note that accounting for the absorption in air does not influence the results very much. For example, if we assume α=0 in the foregoing calculations, then $\varepsilon_1 = -875+i\cdot615$. Inaccuracy in measurements of *L* has a small effect on the result of calculations too: 1% deviation in *L* involves 0.5% changes both in $\varepsilon_1^{'}$ and $\varepsilon_1^{''}$. But inaccuracy in δ measurements is much more significant: 1% deviation in δ brings about 0.5% change in $\varepsilon_1^{'}$ and nearly 2% in $\varepsilon_1^{''}$.

The result obtained for ε_1 is very far from that calculated by the Drude model for metal permittivity: with the damping frequency $\nu_\tau=215$ cm^{-1} and the plasma frequency $\nu_p=72800$ cm^{-1} for gold[46] we get $\varepsilon_1^{'}=-101641$ and $\varepsilon_1^{''} = 284090$ at λ=130 μm.

[45] Dragoman M., and Dragoman D. Plasmonics: applications to nanoscale terahertz and optical devices // Prog. Quantum Electron., 2008, v.32, p.1-41.

[46] Ordal M.A., Bell R.J., Alexander R.W., Long L.L., and Querry M.R. Optical Properties of Fourteen Metals in the Infrared and Far Infrared: Al, Co, Cu, Au, Fe, Pb, Mo, Ni, Pd, Pt, Ag, Ti, *V*, and W // Appl. Opt., 1985, v.24(24), p.4493- 4499.

The quantities L and δ for SPP on a gold sample with such ε_1 equal 126 cm and 4.8 mm, respectively. The difference in the experimentally determined and theoretical values for ε_1' and ε_1'' is striking at first sight, but in our opinion it reflects the difference in the optical properties of surface and bulk regions of gold, let alone that it was not crystal but thermally evaporated in our case.

III. Phase-amplitude SPP spectroscopy at THz frequencies

Optical phase-amplitude spectroscopy, called sometimes a dispersive or dielectric spectroscopy, enables scientists to determine spectra of both the absorption coefficient and the refractive index[47]. This kind of SPP spectroscopy implies measurements of the SPP intensity change and its phase shift as a result of the wave interaction with the sample, i.e. whether the bare metal surface or the surface with a layer under study. In other words, such measurements should bring us values of the both parts of the SPP complex refractive index $\kappa=\kappa'+i\cdot\kappa''$. Once one has determined κ' and κ'' he can calculate (solving a corresponding SPP dispersion equation) the dielectric function of the metal ε_1 in case of two-layer wave guiding structure (metal-air) or two parameters (thickness or optical constants) of the layer deposited on the conducting surface in case of three-layer structure [4].

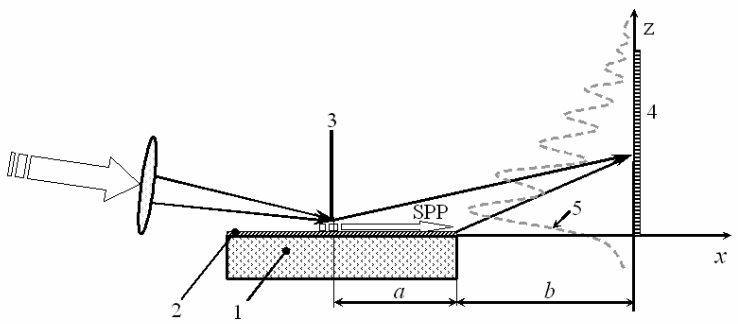

Fig. 13. Sketch of the IR SPP interferometer: 1 – metal specimen; 2 –layer under study; 3 – screen with its edge spaced from the specimen surface by a distance of about 10λ; 4 – detector array; 5 – registered interferogram.

As far as κ'' is concerned there is no much choice for techniques of its determination: in that or another way the SPP intensity has to be estimated in at least two points of the track. But for κ' determination there is a selection: its value may be found whether by amplitude, compensatory or interferometric measurements. Evidently the last-named two techniques are more precise as phase measurements are more accu-

[47] Birch J.R., Parker T.J. Dispersive Fourier Transform Spectroscopy // Infrared and Millimeter Waves, New York: Academic Press, Inc. 1977, v.2, p.137–271.

rate as compared with intensity ones. That is why the first step on the way of the phase-amplitude SPP spectroscopy realization was to develop various types of SPP interferometers.

The principle idea of IR SPP interferometer was first suggested in [28] and represents itself a modified Michelson interferometer in which monochromatic radiation in one of its shoulders exists (part of its path) in the form of SPP accumulating information about the surface. The information is stored in the interference pattern formed by two bulk waves: the reference one and the wave produced by the SPP due to its diffraction at the specimen edge (Fig.13). The interferogram is registered by detector array 4 placed along the axis z at a distance b from the edge.

However, precision of measurements with such interferometer was found to be rather low as (i) the beams interfere at a large angle, making the period of the pattern comparable with the wavelength; (ii) the pattern depends on the features of the diffraction elements (the screen edge, transforming the incident radiation in SPP and generating the first bulk wave, and the specimen edge, transforming SPP into the second bulk wave); and (iii) the wave fronts of the interfering waves significantly differ from planar ones, as a result of which the period and contrast of the interference pattern decrees with an increase in the distance from a sensitive element of array 4 to the specimen surface; let alone the parasitic Lloyd interference due to reflection of the illuminated by the incident radiation screen edge and creation of its bright image into the specimen surface.

It is well known that accuracy of interference measurements is inversely proportional to the convergence angle of the interfering beams. This evidence made us think about a SPP interferometer assuming interference in parallel beams. As SPP field at THz frequencies extends into air over a distance of several centimeters (reducing its intensity by the $e \approx 2.718$ factor) they can be treated like plane waves in interference and plane mirror reflection processes[48]. Therefore there are three possibilities for realizing a SPP interferometer in parallel beams: a) interference of two bulk beams, one

[48] Bell R.J., Goben C.A., Davarpanah M. et al. Two-dimensional optics with surface electromagnetic waves // Appl. Optics, 1975, v.14 (6), p.1322-1325.

of which is produced by SPP; b) interference of two SPP beams; c) interference of SPP and bulk beams.

III.1. ***Phase-amplitude SPP measurements in monochromatic light***

III.1.1. *SPP interferometer with parallel interacting bulk beams*

First THz SPP spectrometer forming its interference pattern in parallel bulk beams was patented in 2008[49]. The new technique enables one to avoid all the drawbacks inherent to interference in converging bulk beams, but we have to "pay the price" for it by increasing the measurements duration in order to register the detector illumination at a number of distances passed by SPP. Scheme of an interferometer employing interaction of two parallel bulk beams is displayed in Fig.14.

There are two specific features in this scheme. Firstly, the specimen surface, guiding SPP, has two conjugated facets, joined by a rib rounded off with a radius $R>>\lambda$. One of the facets contains coupling element 3 converting radiation of the source in SPP, while on the other facet, SPP run rather a long distance x to mirror 5 transforming them into bulk waves (BWs). This separation of the transforming elements by placing them on different specimen facets is needed to get rid of idle BWs originating due to diffraction of the incident radiation on element 3. Secondly, to realize the reverse transformation process (from SPP into BWs), plane mirror 5 inclined to the specimen surface is used. Due to inclination the mirror imparts a negative (relative to the SPP propagation direction) impact, making the SPP wave vector smaller than the BWs wave ones, that is sufficient for transforming the SPP into the BWs.

Measurements of the photocurrent I_1 and I_2 should be done at two distances x_1 and x_2 run by the SPP and corresponding to known number N of interference maxima. Then values of κ' and κ'' can be calculated using the following formulae:

$$\kappa' = n + \Delta\varphi/(k_o \cdot \Delta x), \tag{9}$$

$$\kappa'' = \frac{ln(I_1/I_2)}{k_o \cdot \Delta x}, \tag{10}$$

[49] Zhizhin G.N., Nikitin A.K., Balashov A.A., Rijova T.A. THz SPP spectrometer for a conducting surface study // Patent of Russia on invention, 2008. - No. 2318192.

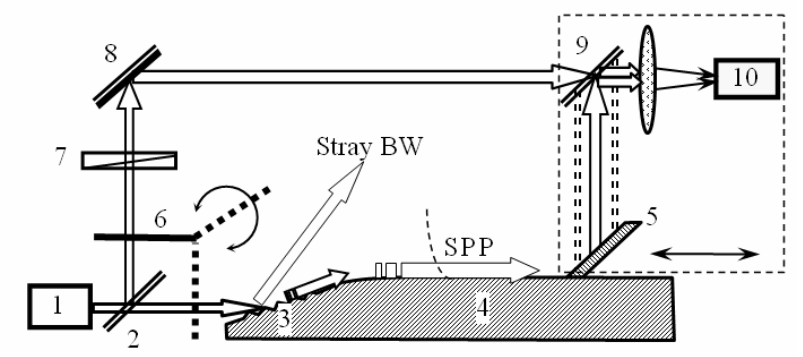

Fig.14. Sketch of SPP interferometer employing interaction of two parallel bulk beams: 1 – tunable source of monochromatic radiation; 2 – beam splitter; 3 - coupling element; 4 – specimen; 5 – moveable mirror; 6 - rotative shutter; 7 – adjustable absorber; 8 – mirror; 9 – beam splitter, conjugated with mirror 5 and photodetector 10 on a mobile platform moving along the specimen surface.

here n is refractive index of air; $\Delta\varphi = N \cdot \pi$ is the phase difference between SPP and the BWs stipulated by the inequality of their phase velocities; $\Delta x = x_2 - x_1$.

Substituting so-obtained κ' and κ'' in the SPP dispersion equation for a three-layer structure [4], one can determine the transition layer optical constants or the dielectric permittivity of the substrate material (metal) for a definite frequency ν.

III.1.2. *SPP interferometer with parallel surface and bulk beams*

It was noted above that SPP at THz frequencies can be treated in many respects like plane waves as their field penetrates into air to a distance of several centimeters. On the other hand, the process of THz SPP excitation by means of incident radiation is attended by unavoidable phantom BWs, overlapping with the SPP field. We combined both these peculiarities of THz SPP and suggested a more simple and effective scheme of a SPP interferometer functioning in parallel beams (Fig.15) [44].

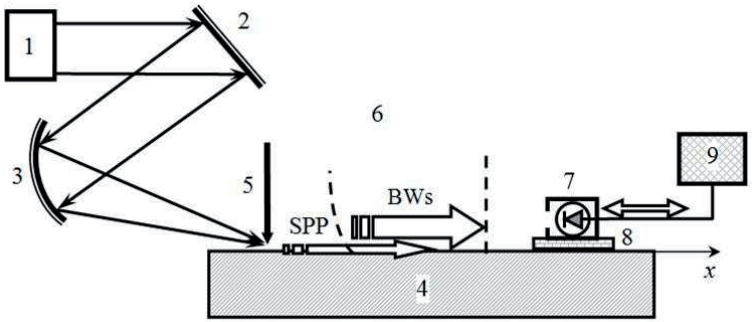

Fig.15. Scheme of the SPP spectrometer employing interaction of surface and bulk waves: 1 – tunable source of monochromatic radiation; 2 – mirror; 3 – focusing mirror; 4 – specimen; 5 – screen with its edge spaced from the specimen surface by a distance of about 10λ; 6 – surrounding medium (air); 7 – photo detector placed on the platform 8, moving along the specimen surface; 9 - data-handling unit.

The spectrometer functions as follows. Using mirrors 2 and 3, radiation of source 1 is directed towards the edge of screen 5, spaced from the specimen plane surface by a controllable distance h. Due to diffraction, the radiation is partially transformed into SPP and BWs, propagating at various angles from the surface. Among this set of BWs there is a beam with a wave vector parallel to the surface and overlapping with the SPP field. The BW and SPP run along the surface with different phase velocities since κ' is larger than the BW refractive index n. As a result of the Joule loses, the SPP intensity decreases exponentially with the absorption factor $\alpha=2k_o\cdot\kappa'$. Having covered the same distance x, the BW and SPP meet detector 7 and acquire phase incursion differing in value by the magnitude $\Delta\varphi= k_o x\cdot(\kappa'-n)$. Being coherent, the BW and SPP interfere and illuminate the detector sensitive element with the intensity I described by the expression:

$$I(x) = I_1 + I_o\cdot\exp(-\alpha\cdot x) + 2\cdot\sqrt{I_1\cdot I_o\cdot\exp(-\alpha\cdot x)}\cdot\cos(\Delta\varphi), \qquad (11)$$

here I_1 is the BW intensity, independent on the distance x; I_o is the SPP intensity right under screen 5 when x=0.

The period Λ of the interference pattern (interferogram) registered by the mobile detector 7 is constant. On measuring Λ, one can estimate the SPP refractive index value from the evident formula:

$$\kappa' = n + \lambda/\Lambda. \tag{12}$$

The SPP absorption index κ'' can be calculated by putting the SPP intensity values measured in two different maxima of the interferogram I_{m1} and I_{m2} in the following formula (its derivation see in Appendix 2):

$$\kappa'' = \frac{2 \cdot ln\left(\frac{\sqrt{I_{m1}} - \sqrt{I_1}}{\sqrt{I_{m2}} - \sqrt{I_1}}\right)}{k_o \cdot (x_2 - x_1)}, \tag{13}$$

here x_1 and x_2 are the coordinates of corresponding maxima, $x_2 > x_1$.

On putting the found values of κ' and κ'' in the SPP dispersion equation for a three-layer structure[4], unit 9 computes two parameters of the structure: both the thickness and refractive index of the transition layer or the complex dielectric permittivity of the metal. Note that the contrast of the interferogram can be controlled by changing the distance h from the screen edge to the specimen surface.

To illustrate the technique of THz SPP amplitude-phase spectroscopy in parallel surface and bulk beams let us consider the following example. Suppose we have to determine dielectric permittivity of aluminum (*Al*) at λ=100 μm using the method. To reduce L below 30 cm the metal surface is covered with a uniform layer of germanium (*Ge*) 0.7 μm thick. Assume that the screen converting radiation of the source into SPP is placed at the distance h ensuring equality $I_1 = I_o$, i.e. the intensity of the BW propagating parallel to the surface equals the SPP intensity under the screen. The surrounding medium is air (n=1.00027).

The calculated dependence $I(x)$ for the interferogram in this case is depicted in Fig16. We carried out the calculations using the Drude model for dielectric permittivity of metals, assigning that the frequencies of plasma ν_p and free electron collision ν_τ for *Al* are equal to 660 cm^{-1} and 119000 cm^{-1}, accordingly[50].

[50] Ordal M.A., Long L.L., Bell R.J. et al. Optical properties of the metals Al, Co, Cu, Au, Fe, Pb, Ni, Pd, Pt, Ag, Ti and W in the infrared and far infrared // Appl. Optics, 1983, v.22(7), p.1099-1119.

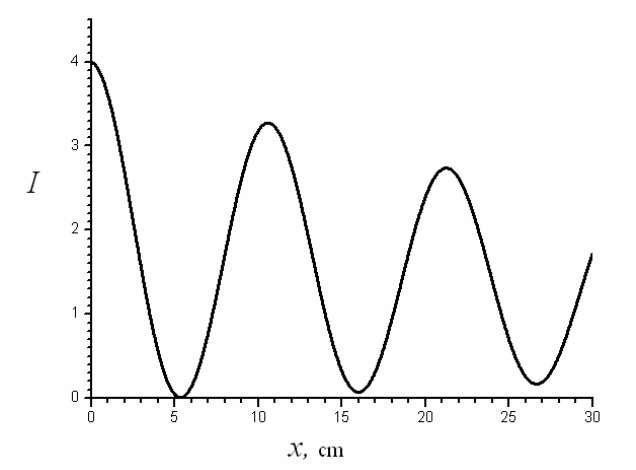

Fig.16. Interferogram, calculated for the structure "*Al – Ge* layer 0.7 ?m thick - air" at λ=100 μm.

Having registered such an interferogram by moving detector 7, one can determine both κ′ and κ″. For example, from the graph presented it follows that: 1) the interferogram period Λ=10.675 cm, which according to (12) corresponds to κ′=1.00121; 2) the resulting intensities in the first I_{m1} and the second I_{m2} maxima, reached at the distances x_1=10.565 cm and x_2=21.240 cm, are equal to 3.275 and 2.739 accordingly. Putting the values of I_{m1}, I_{m2}, x_1 and x_2 in (13), we get $\kappa''=6.3\cdot10^{-5}$. At the final stage of the execution procedure we can solve the SPP dispersion equation for a three-layer structure relatively to the dielectric permittivity of the metal substrate $\varepsilon_1=\varepsilon_1^{'}+i\cdot\varepsilon_1^{''}$. Thus in the example considered we obtain that *Al* permittivity at λ=100 μm equals to ε_{Al}=-31780+i·209745. Having done similar measurements and calculations for other radiation wavelengths one can determine the THz spectra $\varepsilon_1^{'}$ and $\varepsilon_1^{''}$ of the metal.

It is worth noting that both techniques considered in paragraphs III.1.1 and III.1.2 may be used to realize THz SPP Fourier-transform spectroscopy in case the incident radiation has a continuous spectrum.

III.1.3. *SPP interferometer with two quasi parallel surface beams*

In this paragraph, we describe a SPP interferometer based on the concept of asymmetric static interferometry in the planar version, where the interference pattern is formed by converging at a small angle surface rather than bulk waves and interference patterns are recorded in the plane of the specimen surface. As a result, the elements with unknown characteristics (specimen and screen edges) are excluded from measurements. The information about the real part of the SPP refractive index is carried by the interference pattern period, while its imaginary part can be found by mathematical processing of the illumination magnitudes in the pattern extrema.

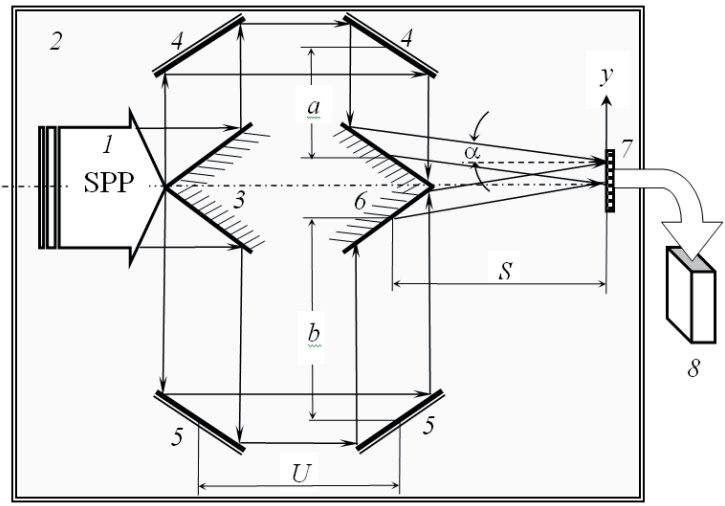

Fig.17. Schematic of the static asymmetric THz SPP interferometer (top view).

Fig. 17 shows the scheme of the developed interferometer: (1) - initial surface-plasmon beam; (2) - sample; (3) - corner mirror, splitting the initial beam into two coherent beams; (4, 5) – mirrors reflecting the surface-plasmon beams in the first and second arms of the interferometer; (6) - second corner mirror, converging both surface-plasmon beams; (7) - line of photodetectors; and (8) - computational device. All mirrors are placed on the surface of sample 2 and oriented perpendicularly to it.

The interferometer works as follows. Initial SPP beam 1 with width *w* is guided by the surface of specimen 2 and reaches the first corner mirror 3, which splits it into

two coherent SPP beams, propagating perpendicularly to the track of the beam 1 in opposite directions. New SPP beams reach mirrors 4 and 5, pair wise located at distances *a* and *b* from the plane of incidence, reflect from them, and arrive at the adjacent faces of the second corner mirror 6, whose faces are oriented so as to make the reflected beams fall at angle α on photodetector array 7. The SPP beams, transmitted at different distances along the specimen surface, form an interference pattern with the period Λ, which is recorded by array 7. Device 8, using the electric signals from array 7 and the known coordinates of its elements, determines Λ and estimates luminance in the interference pattern extrema. Whereupon, on the basis of these results, device 8 calculates both parts of the complex refractive index of the SPP.

In accordance to the interference theory[51], the pattern spatial period Λ is related to κ' as:

$$\kappa' = \lambda/(2\Lambda\sin\alpha). \qquad (14)$$

The radiation intensity distribution $I(y)$ on array *7*, on the assumption of planar wave fronts of the SPP interfering beams, has the form:

$$I(y,k_o) = I_{bg} + I_{interf.}, \qquad (15)$$

here:

I_{bg} is the background term:

$$I_{bg} = I_o \cdot D \cdot exp[-2k_o \cdot \kappa''(U+S/cos\alpha)] \times$$
$$\times \{exp[(-2k_o\kappa'' \cdot (2a+y \cdot sin\alpha)] + exp[-2k_o \cdot \kappa'' \cdot (2b-y \cdot sin\alpha)]\};$$

$I_{interf.}$ is the interference term:

$$I_{interf.} = 2I_o \cdot D \cdot exp[-2k_o\kappa''(U+S/\cos\alpha)] \cdot exp[-2k_o\kappa''(a+b)] \times cos[2k_o\kappa' \cdot (b-a - y \cdot \sin\alpha)];$$

y=0 is the coordinate of the center of the array 7; I_o is the initial beam intensity in the face plane of mirror 3; *U* is the distance between the centers of the beams reflected by mirrors 4 and 5; *S* is the distance between the centers of the beams reflected by the mirror 6 and array 7; *a* and *b* are the half-distances passed by the beams in the directions perpendicular to the initial beam track in the first and second interferometer

[51] Born M., Wolf E. Principles of Optics: Electromagnetic Theory of Propagation, Interference and Diffraction of Light / Cambridge University Press, 1999. - 987 p.

arms; α is the angle between any interfering beam and the initial beam; and *D* is the dynamic (voltage–power) sensitivity of the photodetectors.

On the basis of the interference pattern intensity measurements at points with known *y* coordinates, one can calculate (solving numerically Eq. (15)) the imaginary part κ" of the SPP refractive index.

Note that successful operation of the interferometer implementing the proposed method implies planar wave fronts of the interfering surface waves; this circumstance simplifies treatment of the measurement results. This condition is reliably satisfied in the direction perpendicular to the sample surface, because the vertical size of the photodetectors is much smaller then the penetration depth δ of THz SPP field in air. The SPP wave front in the specimen plane is linear and oriented perpendicularly to the SPP propagation direction as the angular diffraction beam broadening (λ/w) is small (about 10^{-3} rad) due to the fact that the transverse beam size *w* is many times larger than λ [51].

To illustrate the interferometer performance, let us consider its application for determining the refractive index of SPP excited by laser radiation with λ=110 μm on the plane surface of an aluminum specimen in air. The width *w* of the initial surface-plasmon beam will be assumed to be 2.0 cm. The tilt angles of the faces of mirror 3 with respect to the plane of symmetry of the initial beam are chosen to be 45°, and similar angles of the mirror 6 are 47°00′. The pair of mirrors 4, reflecting the surface-plasmon beam in the first interferometer arm, is placed at the distance *a*=2.0 cm from the plane of symmetry of the initial beam, and the pair of mirrors 5, reflecting the surface-plasmon beam in the second interferometer arm, is located at the distance *b*=12.0 cm. The distance *U* between the centers of pairs of mirrors 4 and 5 is taken to be 5.0 cm. Then, the difference in the geometric paths of the first and second beams is 20.0 cm. The distance *S* from the corner mirror 6 to array 7 is chosen to be 15.354 cm, which ensures the angle of beam convergence α=2.0°.

Array *7*, composed of photodetectors with a size of 10 μm, records the interference pattern with the constant period Λ=0.79 mm, whose contrast gradually increases with an increase in the coordinate *y*. The calculated pattern, normalized to the con-

stant $I_o \times D$, is displayed in Fig. 18. Substituting the values of Λ, λ, and angle α into formula (14), one obtains κ' = 1.0008.

Fig. 19 shows the dependence of the ratio $(I_m - I_1)/(I_m + I_1)$ (in percent) on the number of pattern maxima m, where I_m and I_1 are the radiation intensities in the mth and 1st maxima, respectively. For example, this ratio for the 12th maximum is 0.28%, a value corresponding to an excess of I_{12} above I_1 by approximately 0.56%. Such a difference in the intensities is reliably detected by commercial THz detectors[52]. Then, solution of Eq. (15) with the use of the noted values of λ, α, ratio $(I_{12} - I_1)/(I_{12} + I_1)$, and Λ=0.79 mm gives κ" =2? 10^{-4}.

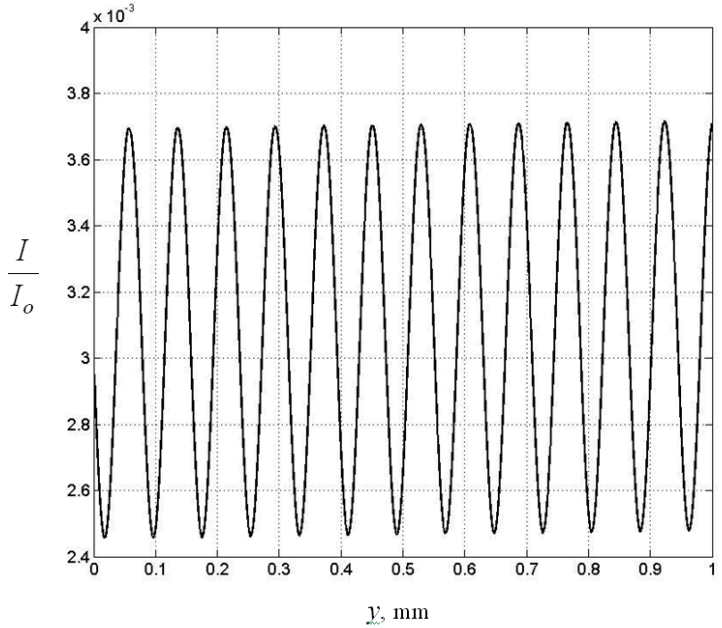

Fig. 18. Calculated interference pattern.

Taking into account that the error in measuring THz intensity by modern detectors is not larger than 10^{-3}%, the stability of λ is about 1%, and, assuming the error in measuring the coordinates of pattern maxima to be 10 ?m, one can find that the errors in determining κ' and κ" by the interferometer are 0.1 and 1%, respectively. These va-

[52] Wolfe W.L., Zissis G.J. The Infrared Handbook / Environmental Research Institute of Michigan, 1985. - 1700 p.

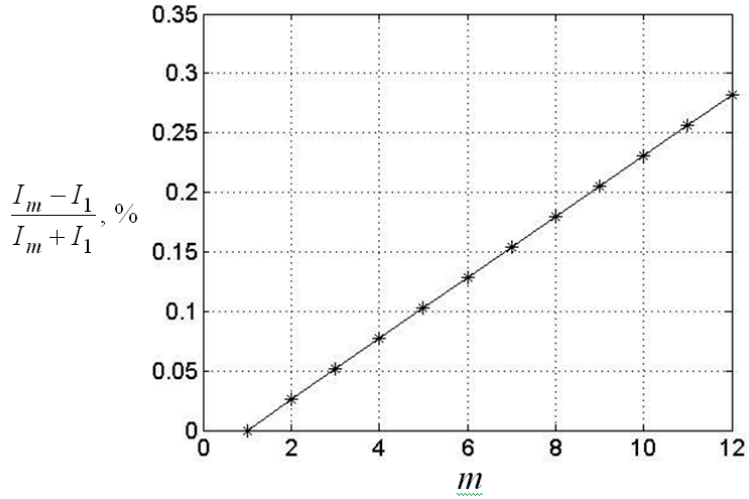

Fig. 19. Dependence of the relative change in the intensity in the interference pattern maxima on the index *m* of the maximum in the considered example of determining the complex refractive index of THz surface plasmons.

lues are an order of magnitude smaller than the errors in determining κ' and κ" when other known methods of SPP refractometry.

Thus, the transition from the interferometry of bulk waves to the interferometry of surface waves and application of the concept of asymmetric interferometry make it possible to reduce not only the error in determining both parts of the complex refractive index of THz SPP but the measurement time (down to the duration of one source pulse) as well.

III.2. ***Phase-amplitude SPP measurements in broad-band THz radiation***

There two main techniques of performing measurements of this kind: 1) Fourier spectroscopy (FS) employing a CW broad-band source like a heated body or a quasi CW intensive pulse source like a synchrotron; 2) time-domain spectroscopy (TDS) employing a picosecond pulses of THz radiation having spectrum spanning the whole THz spectral range. Depending on the type of the source (continuous or pulsed), frequency-domain and time-domain spectroscopies are distinguished.

III.2.1. *Frequency-domain Fourier spectroscopy of bulk samples*

The classical variant of the frequency-domain FS is the amplitude-phase Fourier-transform spectroscopy, which is based on the analysis of an interference pattern that is formed by two parallel beams of broadband radiation one of which interacts with a bulk sample [47]. To extract information on the spectra of amplitudes and phases of the radiation, an interferogram obtained in the course of variation of the path difference between the measuring and reference beams is subjected to a complete (cosine and sine) Fourier transform.

III.2.2. *Time-domain Fourier spectroscopy of bulk samples*

The method of chronospectroscopy (or time-domain spectroscopy; TDS) has become a new stage in the development of FS. This method is based on the measurement of the evolution of the amplitude and phase of a picosecond pulse of THz radiation during its interaction with a bulk object[53]. The TDS method can be implemented upon using femtosecond light flashes to strobe a picosecond pulse of THz waves by multiple switching on (during the pulse) a receiving photoconductive dipole antenna (PDA), current strength I in which is proportional to strength E rather than to the intensity of the radiation to be detected. Having performed an inverse complete Fourier transform of the function $I(t)$, one can obtain frequency spectra of amplitudes and phases of the THz radiation. On obtaining these spectra, one can calculate the spectrum of the complex dielectric permittivity of the sample provided its thickness is known.

The basic merits of the TDS method are the possibility of detecting THz radiation at room temperature (PDA is sensitive only to coherent radiation synchronized with femtosecond pulses) and a large width of the frequency spectrum (several THz), which is inversely proportional to the duration of the THz pulse.

The drawbacks of chronospectroscopy are (i) a long time of measurements because of the necessity of averaging of results over a large number of pulses, which involves severe requirements of synchronism and identity of THz and light pulses;

[53] Grischkowsky D., Keiding S., Exter M., and Fattinger Ch. Far-infrared time-domain spectroscopy with terahertz beams of dielectrics and semiconductors // J. Opt. Soc. Am. (B), 1990, v.7(10), p.2006-2015.

(ii) a limited (compared to laser spectroscopy) spectral resolution, which is inversely proportional to the time of scan of one THz pulse (≈1 ns); and (iii) the dynamic range of TDS systems depends on the frequency of THz radiation (exponentially decreases with its increase). Therefore, the TDS method has its own restrictions and preferable ranges and conditions of application[54].

III.2.3. *Time-domain Fourier spectroscopy of THz surface plasmon-polaritons*

Researchers have attempted to use the TDS method in plasmonic THz spectroscopy[17]. Picosecond THz pulses were converted into SPP by diffraction on the edge of an opaque screen that was brought to the surface of gold that contained a layer under investigation. Having traveled the distance of 1.8 cm, the SPP were transformed by a second screen into bulk radiation, which was detected with a PDA. As well as in the case of bulk samples, the dependence $I(t)$ for a sequence of identical THz pulses was measured by scanning a delay line. It turned out that, in the case of the sample probed by the field of SPP, determination of the amplitude–phase spectra is complicated by the fact that the complex instrumental function acquires additional unknown complex factors, which take into account the transformation efficiency of bulk radiation into SPP and vice versa, as well as the dispersion of the phase shift of radiation components at these transformations. Therefore, the authors of [17] restricted themselves to obtaining the amplitude spectra of the probing THz pulses and to estimating the penetration depth of the SPP field δ into air. Unfortunately, they did not take into account the effect of generation of near surface bulk waves during the diffraction, which are capable of completely skewing the results of the experiments [27, 30].

More informative experiments on thin layers study by the TDS method with excitation of SPP have been described in [55]. It was found that, because of a weak decay of THz SPP and large penetration depth of their field into air, the aperture transformation of the incident radiation into THz SPP on a bare conducting surface is practically

[54] Han P. Y., Tani M., Usami M., Kono S., Kersting R., and Zhang X.-C. A direct comparison between terahertz time-domain spectroscopy and far-infrared Fourier transform spectroscopy // J. Appl. Phys., 2001, v.89(4), p.2357-2359.

[55] Isaac T. H., Barnes W. L., and Hendry E. Determining the terahertz optical properties of subwavelength films using semiconductor surface plasmons // Appl. Phys. Lett., 2008, v.93, 241115.

impossible. To realize the FS of thin layers in the THz range by the SPP spectroscopy method, it was suggested to replace metals with semiconductors, the conductivity of which is much lower compared to metals. Moreover, to obtain the spectra of both parts of the SPP complex refractive index, the authors normalized signals from the PDA in the presence of a layer on the substrate to signals obtained in the absence of this layer. Nevertheless, the results of these experiments are also questionable, since the distance between the apertures (screens), transforming the radiation into SPP and vice versa, was only 1.0 cm, and it was absolutely impossible to avoid falling intense diffraction satellites of the SPP onto the edge of the second screen.

To conclude the discussion of the possibility of realization of plasmon chrono-spectroscopy, we can state that such measurements still bear a preliminary character and, at present, well-reproduced measurement results of characteristics of THz SPP by the TDS method are unavailable yet.

III.2.4. ***Frequency-domain Fourier spectroscopy of THz SPP***

Fourier spectroscopy of THz SPP was first reported by researchers of the Institute for Spectroscopy of the Russian Academy of Sciences[56]. In that work, a globar served as a source of THz radiation; signals were received by a nitrogen-cooled *CdHgTe* detector; and, for transformation elements, diffraction gratings that were separated by a screen and spaced along the surface of a copper sample by a distance of 1.0–1.5 cm, were used. The radiation was focused onto the input element; the spectrum of SPP in the range from 1000 to 1700 cm^{-1} was excited (with various efficiencies). As soon as the SPP beam reached the output element, it was transformed into a set of corresponding diverging bulk waves, which were formed into a collimated beam and directed to the entrance of a Fourier-transform spectrometer. Since the specimen was located prior to the interferometer, the inverse Fourier transform ensured only the amplitude spectrum of the SPP beam, which is described by the imaginary part κ'' of the refractive index of plasmons. The values of κ' were sought from interference patterns formed by a reference beam and a bulk wave generated by the SPP beam dif-

[56] Zhizhin G.N., Yakovlev V.A. Broad-band spectroscopy of surface electromagnetic waves // Physics Reports, 1990, v.194(5-6), p.281-289.

fracting on the sample edge. The drawbacks of this IR SPP Fourier-spectroscopy are separate determination of the spectra of κ' and κ", a low signal-to-noise ratio (due to low spectral intensity of the source and a low excitation efficiency of SPP), and a long measurement time.

We posed the problem of developing basic principles of dispersive Fourier transform spectroscopy of IR SPP, generated by a broadband radiation source, that makes it possible to determine simultaneously the spectra of the both parts of their refractive index in one cycle of measurements. The method should be efficient in studies of the surface of conductors and semiconductors, as well as in measuring the spectra of the dielectric permittivity of thin layers in the far IR range.

III.2.4.1. ***Schematic of asymmetric THz SPP Fourier spectrometer***

Optical scheme of the asymmetric SPP Fourier-transform spectrometer employing continuous radiation and able of determining spectra of the both parts of THz SPP complex refractive index is presented in Fig. 20[57]. It resembles the interferometer presumed for study of monochromatic THz SPP (see Fig. 14), except for it employs a

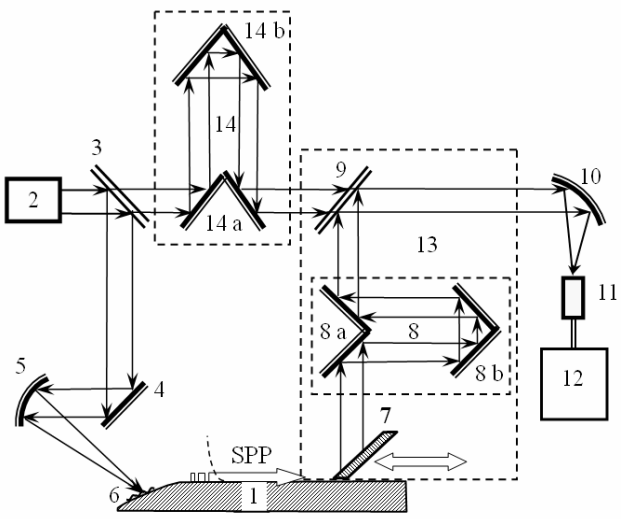

Fig. 20. Schematic of the THz SPP Fourier-transform spectrometer. Details are given in the text.

[57] Zhizhin G.N., Kiryanov A.P., Nikitin A.K., Khitrov O.V. Dispersive Fourier-transform spectroscopy of surface plasmons in the infrared frequency range // Optics and Spectroscopy, 2012, v.112(4), p.545–550.

a broad-band source and two delay lines. A solid specimen 1, which guides SPP, is placed in one of the arms of a Mach–Zehnder interferometer. Collimated radiation emitted by broadband source 2 is incident on beam-splitter 3, which divides it into two beams - a reference beam and a probe beam. Mirrors 4 and 5 focus the probe beam onto an element 6, which transforms the radiation into a beam of SPP with different κ. A set of excited SPP travels a distance a (on the order of L for the maximal frequency of the radiation) to inclined mirror 7, the reflecting surface of which is adjacent to the specimen surface and the lower edge of which is oriented perpendicularly to the SPP track. Mirror 7 imparts a negative impact to all the SPP, as a result of which they are transformed into bulk radiation. This ensures fulfillment of the inequality $k_{SPP} < k_0$, which is necessary to transform SPP into a bulk wave (where k_{SPP} and $k_0=2\pi/\lambda$ are the moduli of the wave vectors of SPP and plane wave in air, respectively). Delay line 8, which consists of fixed 8a and movable 8b corner mirrors, ensures scanning of the optical path length difference $\Delta\ell$ of the interfering beams in the range to $\pm\Delta\ell_{max}$. To expand the dynamic range of measurements, we applied the well known operation of the phase modulation of the light flux in one of the arms of the interferometer by means of harmonic oscillations $\delta\ell(t) = \delta b \cdot \sin(\Omega t)$ of mirror 8b with a cyclic frequency Ω and a small amplitude δb. The beams are superimposed by splitter 9, interfere, and are focused by mirror 10 onto detector 11. Electric signals generated by the detector are fed to the input of information processing unit 12. Note that mirror 7, delay line 8, and beam splitter 9 are mounted on platform 13, which is displaced parallel to the surface of specimen 1. To ensure the coherence of monochromatic components of the beams arriving at beam splitter 9, additional delay line 14 is introduced into the reference channel, which consists of fixed 14a and movable 14b corner mirrors, the axes of which are perpendicular to the surface of specimen 1.

III.2.4.2. ***Theoretical substantiation of THz SPP FT-spectroscopy***

Here we derive relationships that clarify the principle of operation of a Fourier-transform spectrometer by which the spectrum of the complex refractive index of THz surface plasmons can be measured.

The complex amplitudes $\hat{A}_{1\nu}$ and $\hat{A}_{2\nu}$ of the harmonic components of the reference and measuring beams on splitter 9 have the form:

$$\hat{A}_{1\nu} = A_{o\nu} \cdot \hat{\alpha}_{1\nu} \cdot exp[ik_{o\nu} \cdot (C \cdot t - n_\nu \ell_1 - n_\nu \ell_o)], \tag{16}$$

$$\hat{A}_{2\nu} = A_{o\nu} \cdot \hat{\alpha}_{2\nu} \cdot exp\{ik_{o\nu} \cdot [C \cdot t - \kappa_\nu a - n_\nu \cdot (\ell_2 - a) - n_\nu \cdot (\Delta\ell + \delta\ell)]\}. \tag{17}$$

Here, $A_{0\nu}$ is the amplitude of the spectral component with the frequency ν at the entrance of the interferometer; $\hat{\alpha}_{1\nu} = \alpha_{1\nu} \cdot exp(i\varphi_{\alpha 1})$ and $\hat{\alpha}_{2\nu} = \alpha_{2\nu} \cdot exp(i\varphi_{\alpha 2})$ are the complex instrumental functions for the component with the frequency ν in the first (reference) and second (measuring) channels; $\alpha_{1\nu}$, $\alpha_{2\nu}$, and $\varphi_{\alpha 1}$, $\varphi_{\alpha 2}$ are the amplitudes and phases of the instrumental functions; $k_{0\nu} = 2\pi\nu / C = 2\pi\sigma$ is the modulus of the wave vector of the spectral component with the frequency ν; $\sigma = 1/\lambda$ is the wavenumber (cm^{-1}); t is the time; ℓ_1 is the path length of the beam in the reference channel; ℓ_2 is the distance that the measuring beam travels in the air, except for delay line 8; $\Delta\ell$ is the distance that the measuring beam travels in delay line 8; l_0 is the additional distance that the reference beam travels in line 14; a is the distance traveled by the SPP; and n_ν and $\kappa_\nu = \kappa_\nu' + i \cdot \kappa_\nu''$ are the refractive indices of the air and the SPP at the frequency ν, respectively.

Let's rewrite expressions (16) and (17) in the following terms:

$$\hat{A}_{1\nu} = A_{o\nu} \cdot \alpha_{1\nu} \cdot exp(i \cdot \varphi_1), \tag{18}$$

with $\varphi_1 = k_{0\nu} (C \cdot t - n_\nu \cdot \ell_1 - n_\nu \cdot \ell_o) - \varphi_{\alpha 1}$; and

$$\hat{A}_{2\nu} = A_{o\nu} \cdot \alpha_{2\nu} \cdot exp(-k_{0\nu} \cdot \kappa_\nu'' \cdot a) \cdot exp(i \cdot \varphi_2), \tag{19}$$

with $\varphi_2 = k_{0\nu} \cdot [C \cdot t - \kappa_\nu' \cdot a - n_\nu \cdot \ell_2 - n_\nu \cdot (\Delta\ell + \delta\ell)] - \varphi_{\alpha 2}$.

Then the autocorrelation function $\Delta I_{int}(\Delta\ell)_\Omega$ (interferogram) may be written in the form:

$$\Delta I_{int}(\Delta\ell)_\Omega = \int_0^\infty / \hat{A}_{1\nu} + \hat{A}_{2\nu} /^2 \, d\nu. \tag{20}$$

Let's rewrite the integration element of expression (20) in the following terms:

$$| \hat{A}_{1\nu} + \hat{A}_{2\nu} |^2 = \hat{A}_{1\nu} \cdot \hat{A}_{1\nu}^* + \hat{A}_{2\nu} \cdot \hat{A}_{2\nu}^* + (\hat{A}_{1\nu} \cdot \hat{A}_{2\nu}^* + \hat{A}_{1\nu}^* \cdot \hat{A}_{2\nu}), \tag{21}$$

here $\hat{A}_{1\nu}^{\,*}$ and $\hat{A}_{2\nu}^{\,*}$ are complex conjugate values of $\hat{A}_{1\nu}$ and $\hat{A}_{2\nu}$, respectively.

Then, in terms of expressions (18) and (19), one can obtain:

$$\left|\hat{A}_{1\nu}+\hat{A}_{2\nu}\right|^2 = \tag{22}$$
$$= A_{0\nu}^2\cdot\alpha_{1\nu}^2 + A_{0\nu}^2\cdot\alpha_{2\nu}^2\cdot exp\left(-k_{0\nu}\kappa_\nu''\cdot a\right)+ A_{0\nu}^2\cdot\alpha_{1\nu}\cdot\alpha_{2\nu}\cdot exp\left(-k_{0\nu}\kappa_\nu''\cdot a\right)\times$$
$$\times\left\{exp\left[i\cdot(\varphi_1-\varphi_2)\right]+exp\left[-i\cdot(\varphi_1-\varphi_2)\right]\right\}.$$

But employing the Euler formula one can present the expression in the curly brackets as a cosine of the remainder:

$$\left|\hat{A}_{1\nu}+\hat{A}_{2\nu}\right|^2 = A_{0\nu}^2\cdot\alpha_{1\nu}^2 + A_{0\nu}^2\cdot\alpha_{2\nu}^2\cdot exp\left(-2k_{0\nu}\kappa_\nu''\cdot a\right)+$$
$$+2A_{0\nu}^2\cdot\alpha_{1\nu}\cdot\alpha_{2\nu}\cdot exp\left(-k_{0\nu}\kappa_\nu''\cdot a\right)\cdot cos\left(\varphi_1-\varphi_2\right) \tag{23}$$

where $\varphi_1-\varphi_2 = k_{0\nu}\cdot\left(\kappa_\nu'\cdot a+\Delta\ell\right)+\varphi_{oA\nu}+k_{0\nu}\cdot\delta\ell$; $\delta\ell(t) = \delta b\cdot sin(\Omega t)$, $\varphi_{oA\nu}$ is the initial phase difference of the beams of the spectral component with the frequency ν at a minimal optical path length difference $\Delta\ell$ of the beams, which contains the phases of the instrumental functions $\alpha_{1\nu}$ and $\alpha_{2\nu}$.

In this case, for a phase modulated signal, one can get the following expression for cosine of the remainder:

$$cos\left(\varphi_1-\varphi_2\right) = cos\left[k_{0\nu}\cdot\left(\kappa_\nu'\cdot a+\Delta\ell\right)+\varphi_{oA\nu}\right]\times cos\left[k_{0\nu}\cdot\delta b\cdot sin\left(\Omega t\right)\right]-$$
$$-sin\left[k_{0\nu}\cdot\left(\kappa_\nu'\cdot a+\Delta\ell\right)+\varphi_{oA\nu}\right]\times sin\left[k_{0\nu}\cdot\delta b\cdot sin(\Omega t)\right]. \tag{24}$$

There are functions $cos\left[k_{0\nu}\cdot\delta b\cdot sin\left(\Omega t\right)\right]$ and $sin\left[k_{0\nu}\cdot\delta b\cdot sin(\Omega t)\right]$ in the last-named expression. It is obvious that these functions are not harmonic, but periodic ones. That is why they could be expanded into Fourier series:

$$cos\left[k_{0\nu}\cdot\delta b\cdot sin\left(\Omega t\right)\right] = J_0\left(k_{0\nu}\cdot\delta b\right)+2\cdot J_2\left(k_{0\nu}\cdot\delta b\right)\cdot cos\left(2\Omega t\right)+\ldots; \tag{25}$$

$$sin\left[k_{0\nu}\cdot\delta b\cdot sin(\Omega t)\right] = 2\cdot J_1\left(k_{0\nu}\cdot\delta b\right)\cdot sin(\Omega t)+2\cdot J_3\left(k_{0\nu}\cdot\delta b\right)\cdot cos(3\Omega t)\ldots; \tag{26}$$

here $J_n(k_{o\nu}\cdot\delta b)$ is the n-th order Bessel function of the $(k_{o\nu}\cdot\delta b)$ argument.

To eliminate the invariable component the spectroscopic equipment should be adjusted on the first harmonic. That is why the expression (20) can be rewritten in the following form:

$\Delta I_{int}(\Delta\ell)_\Omega =$

$$2\int_0^\infty A_{0\nu}^2\alpha_{1\nu}\alpha_{2\nu}\cdot exp\left(-k_{o\nu}\kappa_\nu''a\right)\cdot J_1\left(k_{o\nu}\delta b\right)\cdot sin\left\{k_{o\nu}\cdot\left[a\cdot\left(\kappa_\nu'-n_\nu\right)+\Delta\ell\right]-\varphi_{oA\nu}\right\}d\nu\,. \qquad (27)$$

Since, in reality, the spectrum of radiation is restricted by a maximal frequency ν_{max}, according to the Kotelnikov sampling theorem[58], integral (27) is replaced by a sum of intensities of discrete monochromatic components with frequencies ν_j over the sampling points $j = 0, 1, 2, \ldots, N$ on the frequency axis,

$\Delta I_{int}(\Delta\ell_m)_\Omega =$

$$2\sum_{j=0}^{N}\left\{\left(A_{0\nu}^2\alpha_{1\nu}\alpha_{2\nu}\right)_j\cdot exp\left(-k_{o\nu j}\cdot\kappa_{\nu j}''\cdot a\right)\cdot J_1\left(k_{o\nu j}\delta b\right)\cdot sin\left\{k_{o\nu j}\cdot\left[a\cdot\left(\kappa_{\nu j}'-n_{\nu j}\right)+\Delta\ell_m\right]-\varphi_{oA\nu j}\right\}\cdot\frac{\nu_{max}}{N}\right\}, \qquad (28)$$

where $\Delta\ell_m$- mth value of $\Delta\ell$ (m =0, 1, 2, …, N) and N is the optimal number of sampling points, which is equal to the resolving power of the Fourier-transform spectrometer [47]:

$$N = 2\cdot(\Delta\ell_{max}\cdot\nu_{max})/C.$$

The application of the inverse complete Fourier transform $\left(\overset{*}{F}\right)$ to the interferogram $\Delta I_{int}(\Delta\ell_m)_\Omega$ yields a complex spectrum of radiation incident on the photodetector, which is described by a sum of the cosine $C_{\nu j}$ and sine $S_{\nu j}$ Fourier transforms of interferogram (28):

$$\left(\overset{*}{F}\right)[\Delta I_{int}(\Delta\ell_m)_\Omega] = C_{\nu j} + i\cdot S_{\nu j}\,. \qquad (29)$$

From complex spectrum (29), one can single out the spectra of its amplitude $A_{\nu j}$ and phase $\varphi_{\nu j}$ components:

$$A_{\nu j} = \sqrt{C_{\nu j}^2 + S_{\nu j}^2} = \left|2\cdot\left(I_{0\nu j}\alpha_{1\nu j}\alpha_{2\nu j}\right)\cdot exp\left(-k_{o\nu j}\kappa_{\nu j}''a\right)\cdot J_1\left(k_{o\nu j}\delta b\right)\right|, \qquad (30)$$

$$\varphi_{\nu j} = Arctg(C_{\nu j}/S_{\nu j}) = k_{o\nu j}\cdot\left(\kappa_{\nu j}'-n_{\nu j}\right)\cdot a+\varphi_{oA\nu j}\,, \qquad (31)$$

[58] Kharkevich A.A. Spectra and Analysis / Russia, Moscow, 2009. – 236 p. (in Russian)

where $I_{0\nu j} = A_{0\nu j}^2$ is the spectral intensity density of the radiation source, $Arctan(x)$ is the principal value of the arctangent in the range $-\pi/2 \le x \le \pi/2$ and is the phase of the complex instrumental function of the instrument at the frequency ν_j.

The spectra $A_{\nu j}$ and $\varphi_{\nu j}$, along with information on the SPP characteristics, also contain information on the complex instrumental function of the instrument, the modulus of which is determined by the amplitude factors $I_{0\nu j}, \alpha_{1\nu j}, \alpha_{2\nu j}$ and $J_1(k_{o\nu j}\delta b)$, and the argument of which is determined by the phase terms $\varphi_{oA\nu j}$. The contribution of all these instrumental parameters can be eliminated by performing measurements for two different path length distances (a_1 and a_2) of the SPP. Having two sets of spectra $A_{\nu j}$ and $\varphi_{\nu j}$, one can find the spectra of $\kappa'(\nu)$ and $\kappa''(\nu)$, using the following relations:

$$\kappa'_{\nu j} = \frac{1}{k_{o\nu j}\Delta a} \cdot \left[Arctg\left(\frac{C_{\nu j}}{S_{\nu j}}\right)_{a_2} - Arctg\left(\frac{C_{\nu j}}{S_{\nu j}}\right)_{a_1} \right] + n_{\nu j}, \tag{32}$$

$$\kappa''_{\nu j} = \frac{1}{k_{o\nu j}\Delta a} \cdot ln \sqrt{\frac{\left(C_{\nu j}^2 + S_{\nu j}^2\right)_{a_1}}{\left(C_{\nu j}^2 + S_{\nu j}^2\right)_{a_2}}}, \tag{33}$$

where $\Delta a = a_2 - a_1$, and the indices "1" and "2" refer to the values of the indexed quantities for the corresponding path length distances of the SPP.

III.2.4.3. *Numerical simulations of the THz SPP Fourier spectrometer functioning*

Let us illustrate the proposed method by an example of determining the spectrum of the complex refractive index of the SPP that are excited on a planar structure "Gold – 1.0 μm *ZnS* layer – vacuum" by broadband radiation with a wavenumber σ varying in the range from 100 to 200 cm^{-1}.

Initially, we calculated the spectra of the real and imaginary parts of the refractive index of the SPP using the SPP dispersion equation for a three-layer structure [4] and the Drude model for the dielectric permittivity of the metal taking into account a weak dispersion of the refractive index of *ZnS*, which is equal to 3.4 in this range.

Then, we numerically simulated interferograms for the two different path lengths of the SPP, a_1=1.0 and a_2=1.5 cm, using a blackbody at temperature of 1000 K, the intensity of which was calculated by the normalized Rayleigh–Jeans formula. The values of a_1 and a_2 were chosen taking into account the condition Δa, a_1, $a_2 \le L_{\min}$ (here, $L_{\min}$=1.8 cm is the propagation length of the SPP for $\sigma_{\max}$=200 cm^{-1}), which ensures the possibility of detecting the signal and determining the complex refractive index of the SPP.

To simplify the calculations, the instrumental function was normalized to the spectral density of radiation with σ=200 cm^{-1}. With the same purpose, the normalized instrumental factors $\alpha_{1\nu}$ and $\alpha_{2\nu}$, as well as the moduli of the normalized coefficients of transformation of bulk waves and vice versa, were taken to be unity.

Fig. 21 presents the central part of a model interferogram, which was calculated at a=a_1 by formula (28) with a resolution of σ_{max}/N = 0.05 cm^{-1} (which corresponds to the total number of sampling points N=4000) for points with m from 1900 to 2100.

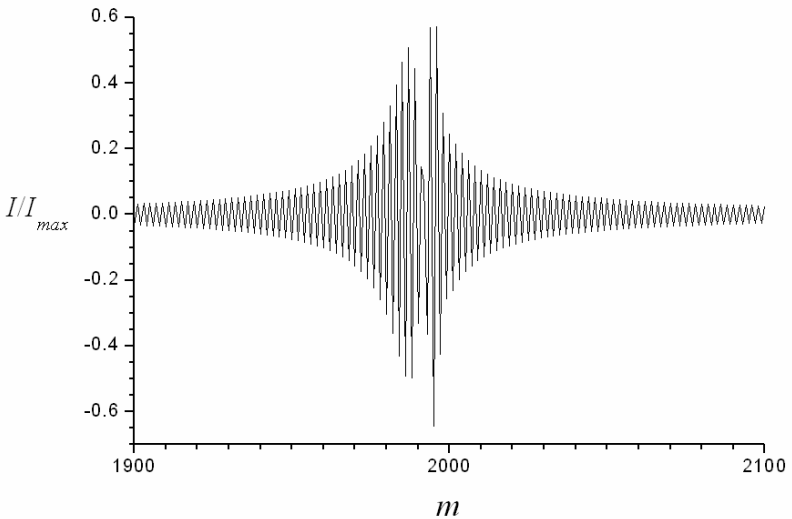

Fig. 21. Simulated interferogram with a resolution of 0.05 cm^{-1} at a=1.0 cm; $I_{\max}$ corresponds to the dynamic range of the instrument.

The Gibbs effect[59], which mainly manifests itself at the ends of the considered range as an increase in the noise of amplitude spectra recovered by the Fourier transform, was suppressed by using an appropriate apodization algorithm[60]. To do this, simulated interferograms were multiplied by the Gauss weight function with the coefficient 2. Further, applying formulas (30) and (31) and the fast Fourier-transform algorithm[61], the amplitude A_{vj} and phase φ_{vj} spectra were recovered. Using relation (33), the spectrum of $\kappa''(\sigma)$ was obtained, which is shown in Fig. 22. The maximal deviation of the recovered spectrum from the simulated one does not exceed 2.5%.

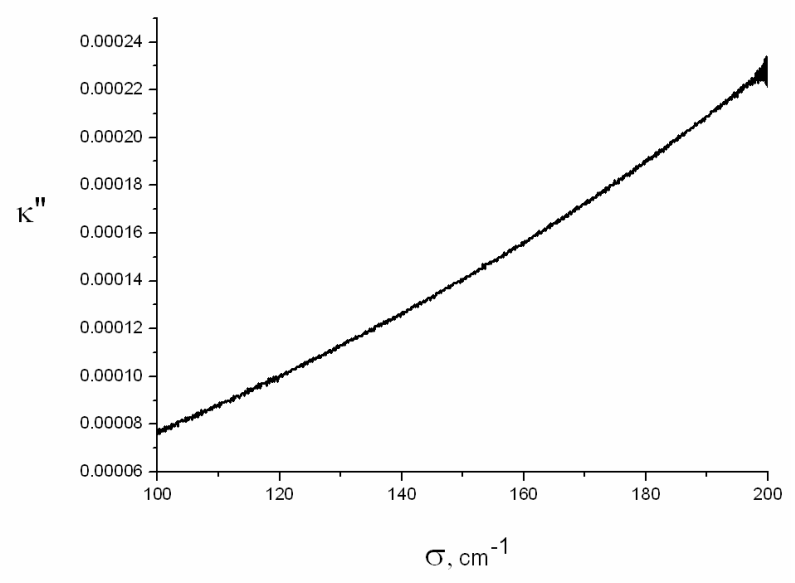

Fig. 22. Recovered spectrum of $\kappa''(\sigma)$.

Upon recovering the spectrum of $\kappa'(\sigma)$ by formula (32), methodological difficulties may arise, which are related to the integer interference order ambiguity for each of the frequency components of the radiation. Since, in the proposed method, the contribution of all instrumental parameters is eliminated by performing measurements at two different propagation lengths of the SPP, the 2π-ambiguity arises only as a result

[59] Methods of Mathematical Physics, 3rd ed. (Cambridge Univ. Press, Cambridge, 1988). – 445 p.
[60] Bell R.J. Introductory Fourier Transform Spectroscopy / University of Missouri-Rolla, USA, 1972. –398p.
[61] Lyons R.G. Understanding Digital Signal Processing / 3rd ed., Prentice Hall, N.Y., USA, 2011. – 954 p.

of the interaction of radiation in the form of SPP with the specimen. Therefore, to eliminate the ambiguity, one can either reduce the spectra φ_{vj}, calculated by formula (16), to the principal value of the arctangent in the range between $-\pi/2$ and $\pi/2$ or

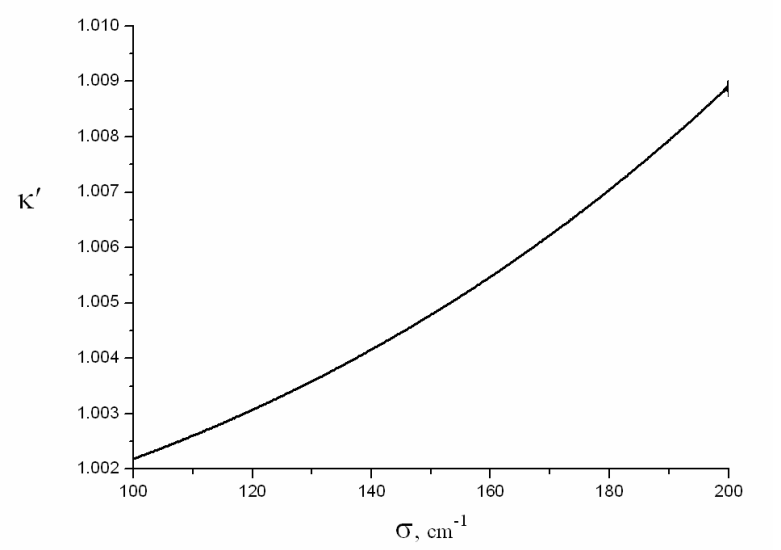

Fig. 23. Recovered spectrum of κ'(σ).

choose $\Delta a = |a_1 - a_2|$ such that it would satisfy the condition $(\kappa'-1)<\lambda_{min}/(2\Delta a)$, at which the accumulated phase difference of the SPP for the minimal wavelength of the work range over the distance Δa does not exceed π.

Fig. 23 shows the recovered spectrum of $\kappa'(\sigma)$. Its maximal deviation from the spectrum that was used upon simulation of the interferogram (see Fig. 22) does not exceed 0.01%.

The considered example of recovering the spectra of $\kappa'(\sigma)$ and $\kappa''(\nu)$ confirms the efficiency of the SPP Fourier-transform spectroscopy method developed for the THz range.

Conclusion

Principles and main points of surface plasmon-polaritons (SPP) spectroscopy in the terahertz (THz) range have been studied and reviewed in this monograph. The SPP spectroscopy enables one to determine the dielectric function of real metal surfaces as well as to investigate sub wavelength layers on such surfaces at THz frequencies. Two kinds of THz SPP spectroscopy are feasible: absorption and amplitude-phase ones. Both of them could be realized whether in dynamic or static regime, but the latter SPP spectroscopy technique enables scientists to determine spectra of both parts of the SPP complex refractive index κ (and thus - complex dielectric permittivity of the surface or its transition layer), while the former – only imaginary part of κ. In spite of some difficulties inherent to excitation and detection of SPP at THz frequencies the method of SPP spectroscopy can be successfully used for study of metal surfaces and thin films in the THz range. The developed method of dispersive Fourier-transform SPP spectroscopy, employing asymmetric Mach–Zehnder interferometers and thermal, synchrotron, or tunable radiation sources (such as free-electron lasers) can be used for studying physicochemical processes on conducting surfaces and for refractometry of metals in the whole far-IR range.

Acknowledgments

The authors express their deep gratitude to Professor Guerman N. Zhizhin, promoter of IR SPP spectroscopy in Russia, for setting the problem of developing THz SPP spectroscopy and for fruitful discussions of the results obtained in the investigations.

Appendix **1**

Formula (8) derivation

According to the definition of the SPP field decay length δ it is related to $\kappa=\kappa'+j\cdot\kappa''$ as follows: $\delta = \left[k_o \cdot Re\left(\sqrt{\kappa^2-\varepsilon_2}\right)\right]^{-1}$. Wherefrom it comes that: $\frac{1}{k_o\cdot\delta} = Re\left(\sqrt{\kappa^2-\varepsilon_2}\right) = A$, where A is a temporary function.

The complex square root may be represented in the trigonometric form:

$$\sqrt{\kappa^2-\varepsilon_2} = \sqrt{\left[(\kappa')^2-(\kappa'')^2-\varepsilon_2'\right]+j\cdot\left[2\kappa'\kappa''-\varepsilon_2''\right]} = \sqrt{\rho}\cdot exp\left(j\cdot\varphi/2\right),$$

here $\rho = \sqrt{\left[(\kappa')^2-(\kappa'')^2-\varepsilon_2'\right]^2+\left[2\kappa'\kappa''-\varepsilon_2''\right]^2}$, $\varphi = atan\left[\frac{2\kappa'\kappa''-\varepsilon_2''}{(\kappa')^2-(\kappa'')^2-\varepsilon_2'}\right]$.

Then:

$$Re\left(\sqrt{\kappa^2-\varepsilon_2}\right) = \sqrt[4]{\left[(\kappa')^2-(\kappa'')^2-\varepsilon_2'\right]^2+\left[2\kappa'\kappa''-\varepsilon_2''\right]^2}\times cos\left\{\frac{1}{2}\cdot atan\left[\frac{2\kappa'\kappa''-\varepsilon_2''}{(\kappa')^2-(\kappa'')^2-\varepsilon_2'}\right]\right\}.$$

On designating $y = \frac{1}{2}\cdot atan\left[\frac{2\kappa'\kappa''-\varepsilon_2''}{(\kappa')^2-(\kappa'')^2-\varepsilon_2'}\right]$ and accounting for $cos(\alpha) = \sqrt{\frac{1+cos(2\alpha)}{2}}$, we get:

$$Re\left(\sqrt{\kappa^2-\varepsilon_2}\right) = \sqrt[4]{\left[(\kappa')^2-(\kappa'')^2-\varepsilon_2'\right]^2+\left[2\kappa'\kappa''-\varepsilon_2''\right]^2}\times\sqrt{\frac{1+cos(2y)}{2}}.$$

Substituting the expression for y in the last equation and taking into account the relation $cos[atan(z)] = \frac{1}{\sqrt{1+z^2}}$ one obtains:

$$Re\left(\sqrt{\kappa^2-\varepsilon_2}\right) =$$

$$\sqrt[4]{\left[(\kappa')^2-(\kappa'')^2-\varepsilon_2'\right]^2+\left[2\kappa'\kappa''-\varepsilon_2''\right]^2}\times\frac{1}{\sqrt{2}}\times\sqrt{1+\frac{1}{\sqrt{1+\left[\frac{2\kappa'\kappa''-\varepsilon_2''}{(\kappa')^2-(\kappa'')^2-\varepsilon_2'}\right]^2}}} =$$

$$= \sqrt{\frac{(\kappa')^2 - (\kappa'')^2 - \varepsilon_2' + \sqrt{\left[(\kappa')^2 - (\kappa'')^2 - \varepsilon_2'\right]^2 + \left[2\kappa'\kappa'' - \varepsilon_2''\right]^2}}{2}}. \qquad (*)$$

Eq. (*) has to be solved relative to κ′. To do this let us introduce the following notations: $a = (\kappa')^2 - (\kappa'')^2 - \varepsilon_2'$ and $b = 2\kappa'\kappa'' - \varepsilon_2''$.

Then eq.(*), in view of the notation for the temporary function *A* (see above), acquires the following form:

$2A^2 = a + \sqrt{a^2 + b^2}$, whence it appears: $4A^4 - 4A^2 a + a^2 = a^2 + b^2$.

On substituting *a* and *b* terms, one can get:

$$4A^4 - 4A^2 \cdot (\kappa')^2 + 4A^2 \cdot (\kappa'')^2 + 4A^2 \cdot \varepsilon_2' = 4(\kappa')^2 \cdot (\kappa'')^2 - 4\kappa'\kappa'' \cdot \varepsilon_2'' + \left(\varepsilon_2''\right)^2.$$

Similar terms bunched, the relation attains the form of quadratic equation:

$$4\left[A^2 + (\kappa'')^2\right] \cdot (\kappa')^2 - 4\kappa'' \cdot \left(\varepsilon_2''\right) \cdot \kappa' - \left[4A^4 + 4A^2 \cdot (\kappa'')^2 + 4A^2 \cdot \varepsilon_2' - \left(\varepsilon_2''\right)^2\right] = 0.$$

The roots of this equation are the following:

$$\kappa' = \frac{2\kappa'' \cdot \varepsilon_2'' \pm \sqrt{4(\kappa'')^2 \cdot \left(\varepsilon_2''\right)^2 + 4\left[A^2 + (\kappa'')^2\right] \cdot \left[4A^4 + 4A^2 \cdot (\kappa'')^2 + 4A^2 \cdot \varepsilon_2' - \left(\varepsilon_2''\right)^2\right]}}{4\left[A^2 + (\kappa'')^2\right]}. \qquad (**)$$

The root with minus must be reject as it corresponds to a negative value of κ′.

To check the validity of eq.(**) we may set $\varepsilon_2'' = 0$ and will obtain eq.(10) from Ref.[44], where the medium adjacent to the sample surface was supposed to have no absorption.

On substituting the expression for $A = \frac{1}{k_o \cdot \delta}$ in eq.(**) one gets desired relation (8):

$$\kappa' = \frac{k_o^2 \delta^2 \kappa'' \varepsilon_2''}{2 \cdot \left[1 + k_o^2 \delta^2 \cdot (\kappa'')^2\right]} + \sqrt{\frac{1}{1 + k_o^2 \delta^2 \cdot (\kappa'')^2}} \times \left[\frac{1}{k_o^2 \delta^2} + (\kappa'')^2 + \varepsilon_2' - \frac{k_o^2 \delta^2 \cdot \left(\varepsilon_2''\right)^2}{4 \cdot \left[1 + k_o^2 \delta^2 \cdot (\kappa'')^2\right]}\right].$$

Appendix **2**

Formula (13) derivation

Suppose we have measured intensity I_{m1} and I_{m2} in two maxima of the interference pattern corresponding to distances x_1 and x_2 run by the SPP. With regard to the fact that for maxima $\Delta\varphi=2\pi b$ (here b – is an integer) these intensities in accordance with formula (7) may be described as follows:

$$I_{m1} = I_1 + I_{21} + 2\sqrt{I_1 \cdot I_{21}} \quad \text{and} \quad I_{m2} = I_1 + I_{22} + 2\sqrt{I_1 \cdot I_{22}},$$

here I_1 – is intensity of the bulk wave, I_{21} and I_{22} – are intensities of the SPP at coordinates x_1 and x_2.

Solving these equations relatively I_{21} and I_{22} we get: $I_{21}=\left(\sqrt{I_{m1}}-\sqrt{I_1}\right)^2$ and $I_{22} = \left(\sqrt{I_{m2}}-\sqrt{I_1}\right)^2$. In view of the exponential SPP field decay we can express I_{22} through I_{21} on assumption that $x_1<x_2$: $I_{22} = I_{21}\cdot exp(-\alpha\cdot\Delta x)$, here $\alpha = k_o\cdot\kappa''$ - is the SPP absorption coefficient, $\Delta x=x_2-x_1$. Wherefrom it follows that: $\alpha\cdot\Delta x = ln\left(I_{21}/I_{22}\right)$. Substituting the expressions for I_{21}, I_{22} and α in the last equation we get the required formula (13).